

NRG Ljubljana  
*User's manual*  
<http://auger.ijs.si/ljubljana>

Rok Žitko  
rok.zitko@ijs.si  
“Jožef Stefan” Institute and  
Faculty for mathematics and physics, University of Ljubljana,  
Ljubljana, Slovenia

January 19, 2007



Framework "NRG Ljubljana" is a set of interrelated computer codes for performing numerical renormalization group (NRG) calculations for quantum impurity problems, described by models such as the Kondo exchange (s-d) model or the Anderson single impurity model, and their multi-impurity and multi-channel generalizations. It also contains a number of tools for analyzing results (thermodynamic properties, such as magnetic and charge susceptibility, entropy and heat capacity; expectation values of arbitrary operators; spectral functions). It is user friendly, in the sense that it is easy to set up new types of problems (Hamiltonians, perturbation terms, etc.) and the output is formatted and annotated for easy interpretation, parsing and plotting.

To achieve a high degree of flexibility without sacrificing numerical efficiency, "Ljubljana NRG" is composed of a hierarchy of modules: high level modules are written in a mixture of functional and procedural Mathematica code, while the low level numerically intensive parts are programmed in the object oriented approach in the C++ language. The foundation of the framework is a Mathematica package for performing calculations with non-commutative second quantization operators, SNEG. Next layer is a Mathematica program which defines the Hamiltonian, the basis of states, and the physical operators of interest: with the help of SNEG, Hamiltonian and operators can be defined using the familiar second-quantization expressions. This program performs the diagonalization of the initial Hamiltonian and prepares the input for the NRG iteration proper.

For efficiency, NRG iteration is performed by a separate C++ program: for a typical problem, most of the time (90%) is spent in the LAPACK `dsyev` or `dsyevr` routine which solves the eigenvalue problem. There is very little housekeeping overhead due to the tasks required by the NRG iteration; "NRG Ljubljana" is thus suitable for performing large scale NRG calculations on computer clusters.

Chapter 1 is a general introduction to the numerical renormalization group based on a chapter from my PhD dissertation. Chapter 2 is the reference manual for the software itself.

"NRG Ljubljana" and this manual are both work in progress. Any comments, critiques, feature request are very welcome.

Rok Žitko

## Acknowledgements

The "NRG Ljubljana" framework is being developed during author's PhD studies at the Faculty for mathematics and physics of the University of Ljubljana, and the "Jožef Stefan" Institute, Ljubljana, Slovenia. Discussions and collaboration with prof. Janez Bonča, prof. Anton Ramšak, Jernej Mravlje and dr. Tomaž Rejec from the F1, Theoretical Physics department are acknowledged.

# Chapter 1

## Numerical renormalization group

The numerical renormalization group (NRG) is a non-perturbative RG approach to the quantum impurity problems.<sup>1-4</sup> Being non-perturbative, it does not suffer from logarithmic singularities, as scaling approaches do. NRG builds upon the RG approach to the Kondo problem of Anderson, Yuval and Hamann,<sup>5-8</sup> however in NRG the RG transformations are performed numerically. The essential advantage of this approach is that the calculation need not be guided by “physical intuition” and is therefore unbiased; however, by the same token there is no straight-forward description in terms of running coupling constants to provide a simple physical picture.

Schematically, NRG consists of logarithmic discretization of the conduction band(s) and of iterative diagonalisation of a series of Hamiltonians. The method was expounded in K. G. Wilson’s seminal paper “The renormalization group: Critical phenomena and the Kondo problem” (Rev. Mod. Phys., 1975)<sup>1</sup> where it was applied to numerically solve the Kondo problem. This was a turning point in the field of impurity problems since an essentially exact solution for the temperature dependence of the thermodynamic quantities in the cross-over region between the high-temperature local-moment regime and the low-temperature strong-coupling regime was obtained for the first time.

NRG has since then become the principal tool in the field of the quantum impurity physics. The approach was used to study the potential scattering in the Kondo problem,<sup>9,10</sup> the s-d problem with spin 1,<sup>11-13</sup> the two-channel Kondo problem,<sup>14-18</sup> particle-hole symmetric<sup>2,19</sup> and asymmetric<sup>3</sup> Anderson model, orbitally degenerate Anderson model<sup>20-23</sup> and models where different magnetic configurations are mixed.<sup>24</sup> More complex multi-impurity problems are also tractable: significant effort was devoted to the two-impurity Kondo problem,<sup>25-28</sup> two-impurity Anderson model<sup>29,30</sup> and, more recently, to clusters of three and more Anderson impurities.<sup>31,32</sup> In addition, local phonon modes can also be taken into account as in the Anderson-Holstein model.<sup>33-37</sup> New direction are applications of NRG to quantum impurity problems with bosonic continuum bath,<sup>38</sup> non-trivial density of states (pseudo-gap) of the conduction band,<sup>39-44</sup> non-Fermi liquid fixed points,<sup>45-48</sup> magnetic impurities in superconductors<sup>49,50</sup> and quantum phase transitions.<sup>51,52</sup> Recently, NRG has become widely applied to study conductance through single,<sup>53-56</sup> double,<sup>57-66</sup> triple<sup>31,32,67</sup> and multiple quantum dots,<sup>68,69</sup> including quantum dots attached to ferromagnetic leads,<sup>70,71</sup> and to study singlet-triplet transitions.<sup>72-75</sup> A number of exotic Kondo states were found, among them the SU(4) Kondo effect.<sup>76</sup>

NRG is increasingly often applied as the impurity solver in the dynamical mean-field theory (DMFT) approach<sup>4,77,78</sup> to lattice problems; notable examples are applications to the Hubbard model,<sup>79</sup> the periodic Anderson model,<sup>80</sup> the Hubbard-Holstein model<sup>81,82</sup> and the two-band Hubbard model.<sup>83</sup>

## 1.1 Implementation overview

“NRG Ljubljana” code was designed and implemented from scratch. The main design goals were flexibility in setting up new problems, ease of taking into account various symmetries, and speed. The code was implemented in a layered architecture, see Fig. 1.1. The cornerstone is a *Mathematica* package `sneg` for performing calculations with second quantization operators. This package is used, on one hand, in deriving the recursion relations for the NRG iteration and, on the other hand, for exactly diagonalizing the initial Hamiltonian and transforming the matrices of all operators of interest in the basis of eigenstates of the Hamiltonian in each invariant subspace. The NRG iteration routines are implemented in C++ for speed. Diagonalisations are performed using `dsevev` and `dsevevr` routines from the LAPACK library,<sup>84</sup> while all other matrix and vector operations use the `ublas` library from the project `boost`. Standard Template Library containers are heavily used, which makes the code easy to read (and maintain) and helps avoid memory leaks. Additional information can be found on the “NRG Ljubljana” home page <http://auger.ijs.si/ljubljana>. The package was released freely for general use under the GNU Public license.<sup>85</sup>

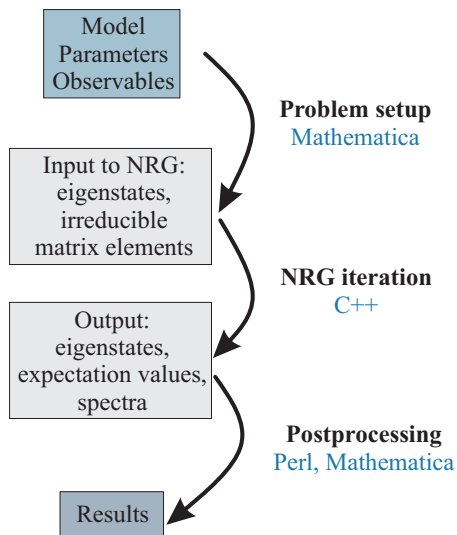


Figure 1.1: The three-step procedure from the problem definition to the results in “NRG Ljubljana” code.

### 1.1.1 Package `sneg`

Package `sneg` is a collection of transformation rules for *Mathematica*, which simplifies calculations using the anti-commuting fermionic second quantization operators. The foundation is a definition of non-commutative multiplication with automatic reordering of operators in a standard form (normal ordering with creation operators preceding the annihilation operators), which takes into account selected (anti-)commutation rules. Standard form reordering allows simplification of expressions and the choice of normal ordering permits efficient evaluation of matrix elements in a given basis. Some of the additional capabilities of the package that are relevant to the NRG code are:

- Generation of basis states with well-defined number  $Q$  and spin  $S$  (or other quantum numbers).
- Generation of matrix representations of operators (in particular of the Hamiltonian) in selected basis.

- Collection of functions that generate various operator expressions, such as electron number, electron spin and isospin, one-electron and two-electron hopping, exchange interaction, etc.
- Occupation-number representation of states and evaluation of operator-vector expressions.

Among miscellaneous features of the package are manipulation routines for operator expressions (canonic conjugation, spin inversion), calculation of vacuum expectation values of operator expressions, transformations from product-of-operators to occupation-number representations of states and vice-versa, Dirac’s bra-ket notation, simplifications using Wick’s theorem, support for sums over dummy indexes (momentum, spin) and simplifications of such expressions, etc. Package `sneg` is useful beyond NRG calculations. It has been applied to perform exact diagonalizations on Hubbard clusters, perturbation theory to higher orders<sup>69</sup> and calculation of commutators of complex operator expressions. It should also be suitable for educational purposes, since it makes otherwise tedious calculations a routine operation: the nicest feature is perhaps that the use of the package prevents inauspicious sign errors when commuting fermionic operators. Package `sneg` was also released freely for general use under the GNU Public license (<http://auger.ijs.si/ljubljana/sneg>).

## 1.2 Logarithmic discretization

The essential element of the NRG approach is the logarithmic discretization of the conduction band whereby the infinite number of the continuum degrees of freedom is reduced to a finite number; this renders the numerical computation tractable. If we attempted to discretize the band linearly, we would obtain a single interval centered around  $k = 0$  that would contain an infinite number of different energy *scales*: this is undesirable, since it is known that in the Kondo problem excitations at each energy scale contribute equally. It is thus preferable to perform a discretization which divides the band into a set of different energy scales; in this manner the energy-scale separation – a known property of QIMs – is achieved explicitly. Viewed from another perspective, the logarithmic mesh gives a good sampling of the states near the Fermi energy which play an essential role in the Kondo problem. Wilson’s logarithmic discretization consists of the following steps:<sup>1,2</sup>

1. The conduction band is divided into slices of exponentially decreasing width, for example into intervals  $I_m^- = [-\Lambda^{-m}, -\Lambda^{-(m+1)}]D$  for holes and  $I_m^+ = [\Lambda^{-(m+1)}, \Lambda^{-m}]D$  for electrons with  $m \geq 0$ , see Fig. 1.  $\Lambda > 1$  is called the *logarithmic discretization parameter* (parameter `Lambda` in “NRG Ljubljana”). An upper bound of  $\Lambda = 3$  has been established for reliable computation of thermodynamic properties in this discretization scheme.<sup>1,86</sup>
2. Each interval is Fourier-transformed, i.e. we construct a complete set of wave functions  $\psi_{ml}^\pm$

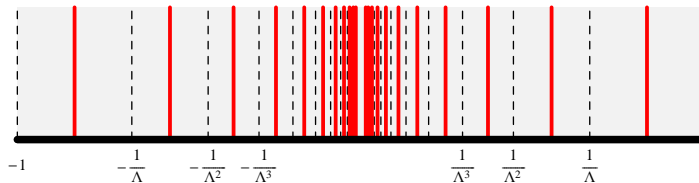


Figure 1.2: Original Wilson’s division of the conduction band into bins of geometrically decreasing width. Each thick colored line corresponds to a state which represents the entire interval of conduction band states delimited by a pair of dashed lines.

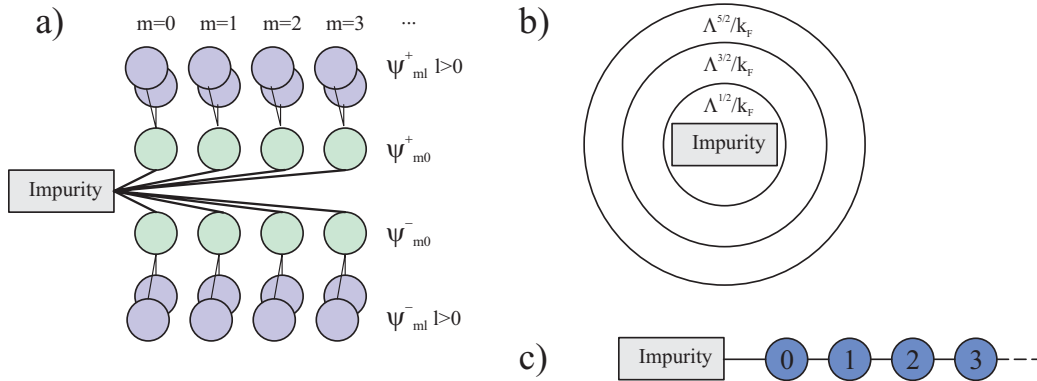


Figure 1.3: Various representation of the logarithmic discretization in quantum impurity problems. **a)** Discretized problem and coupling connectivity of wave-functions  $\psi_{ml}^{\pm}$ . **b)** Onion-shell representation of Wannier orbitals around the impurity. **c)** Hopping or Wilson chain Hamiltonian.

inside each interval:

$$\psi_{ml}^+(\epsilon) = \sqrt{\frac{\omega_m}{2\pi}} \exp(i\omega_m l \epsilon), \quad \text{for } \epsilon \in I_m^+, \quad (1.1)$$

where  $\omega_m$  is the fundamental Fourier frequency in the  $m$ th interval,  $\omega_m = 2\pi\Lambda^m/(1 - \Lambda^{-1})$ , and  $l \geq 0$ . Functions  $\psi_{ml}^-$  are defined similarly for  $\epsilon \in I_m^-$ . The first wave function ( $l = 0$ ) in each interval is a constant. Only such ‘‘average states’’  $\psi_{m0}^{\pm}$  couple to the impurity, while other Fourier components are localized away from it, Fig. 1.3a. We therefore retain only  $\psi_{m0}^{\pm}$  and drop the remaining states from consideration. This is clearly an approximation, since the states  $\psi_{ml}^{\pm}$  couple to  $\psi_{m0}^{\pm}$ . It was shown that this coupling goes to zero as  $\Lambda \rightarrow 1$  (i.e. in the continuum limit) and that even for moderately large  $\Lambda = 2$  up to  $\Lambda = 3$  the approximation is good.<sup>1</sup> Physically, we are neglecting those conduction band states that are localized far away from the impurity in the real space and, at the same time, far away from the Fermi surface in the reciprocal space.<sup>1,87</sup> There is no a priori justification for this approximation; in the words of Wilson: ‘‘The only true justification for using the logarithmic division is that a successful calculation results.’’

- Unitary transformation to a tridiagonal basis is performed using the Lanczos algorithm. The initial state is the Wannier orbital about the impurity site; this is the orbital to which the impurity is coupled in the standard Kondo problem. Lanczos states correspond to creation operators  $f_0^\dagger, f_1^\dagger$  and have a radial extent of  $\Lambda^{1/2}/k_F, \Lambda^{3/2}/k_F, \dots$  about the impurity;<sup>1,15</sup> they form ‘‘onion shells’’ around the impurity, Fig. 1.3b. The conduction band Hamiltonian rewritten in this basis takes the form of a one-dimensional tight-binding model with interacting impurity attached to its end, Fig. 1.3c. This tight-binding Hamiltonian is named the *hopping Hamiltonian* or the *Wilson chain*. The problem is thereby reduced to an effective one dimensional problem. In the  $\Lambda \rightarrow 1$  limit, a continuum model is recovered. It may be noted that the low-energy levels for small  $\Lambda$  are approximately equidistant (as in the field theory defined on a finite-size system), while for moderate  $\Lambda$  the energies are spaced exponentially starting with the third level, Fig. 1.4.
- The total Hamiltonian is defined on an infinitely long chain with exponentially decreasing coupling constants:

$$H = H_{\text{imp}} + H_C + H_{\text{chain}}$$

$$H_{\text{chain}} = \sum_{n=0}^{\infty} \sum_{\mu\alpha} \xi_n \Lambda^{-n/2} (f_{n,\mu\alpha}^\dagger f_{n+1,\mu\alpha} + \text{H.c.}), \quad (1.2)$$

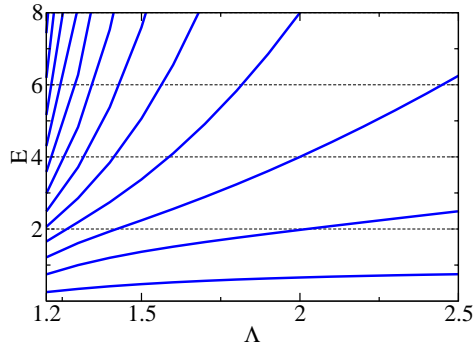


Figure 1.4: Positive one-particle eigenenergies of the Wilson chain Hamiltonian with even number of sites as a function of the discretization parameter  $\Lambda$ .

where  $H_{\text{imp}}$  is the impurity Hamiltonian,  $H_C$  is the coupling Hamiltonian, and  $H_{\text{chain}}$  is the Wilson chain Hamiltonian. In the original Wilson's scheme  $\xi_n$  are correction factors

$$\xi_n = \frac{1 - \Lambda^{-(n+1)}}{[(1 - \Lambda^{-(2n+1)})(1 - \Lambda^{-(2n+3)})]^{1/2}}, \quad (1.3)$$

which rapidly tend to 1. The coupling Hamiltonian  $H_C$  must be rewritten in terms of the Wilson chain operators. In the simplest case of the single-impurity one-channel Kondo problem, it is equal to

$$H_C = JS \cdot \sum_{\mu, \mu'} f_{0, \mu}^\dagger \left( \frac{1}{2} \sigma_{\mu \mu'} \right) f_{0, \mu'}, \quad (1.4)$$

where  $\mathbf{S}$  is the impurity spin operator. It was found that to connect the numerical results at finite  $\Lambda$  to the  $\Lambda \rightarrow 1$  limit, it is necessary to correct the coupling constant  $\Gamma$  (Anderson-model-like coupling) or  $J$  (Kondo-model-like coupling) by multiplying it by a correction factor<sup>2, 88</sup>

$$A_\Lambda = \frac{1}{2} \frac{1 + \Lambda^{-1}}{1 - \Lambda^{-1}} \ln \Lambda. \quad (1.5)$$

This correction can be enabled in “NRG Ljubljana” by setting the option `Alambda` to `true`. While  $A_\Lambda$  is typically small ( $A_2 \approx 1.04$ ,  $A_3 \approx 1.1$ ,  $A_4 \approx 1.16$ ), it must be recalled that  $\Gamma$  or  $J$  enter the exponential function in the expression for the Kondo temperature, therefore  $A_\Lambda$  has a significant effect.

One should keep in mind that for  $\Lambda \neq 1$ , the Hamiltonian obtained from the discretization is only an approximation to the original impurity model and that, strictly speaking, NRG is not an exact method. Nevertheless, by comparing results with known analytical solution (Bethe Ansatz), a remarkable agreement is found. The principal advantage of NRG is its applicability to more complex problems where analytical approaches fail.

Improved discretization schemes are the interleaved method (also known as the “z-trick”)<sup>28, 86, 89</sup> and an approach based on an over-complete basis of states;<sup>90, 91</sup> the latter was found to give excellent results and was used in most of the calculations presented in this work. All three approaches are implemented in “NRG Ljubljana”: the corresponding configuration options are `disc=wilson`, `disc=yoshida` and `disc=campo`, i.e. they are named after the first authors of the publication where they were introduced. In the interleaved method (`disc=yoshida`), the first positive-frequency interval is  $1 > \epsilon > \Lambda^{-z}$ , the others are  $\Lambda^{1-z-m} > \epsilon > \Lambda^{-z-m}$  ( $m = 1, 2, \dots$ ), see Fig. 1.2; for  $z = 1$  this reduces to the original discretization. We then average over the sliding (twist) parameter  $z$  ( $z$  in “NRG Ljubljana”) in the interval  $0 < z \leq 1$  to remove the oscillations in thermodynamic and dynamic quantities which become pronounced for increasing value of parameter  $\Lambda$ .<sup>86</sup> In practice an average over a small number of values of  $z$  already gives

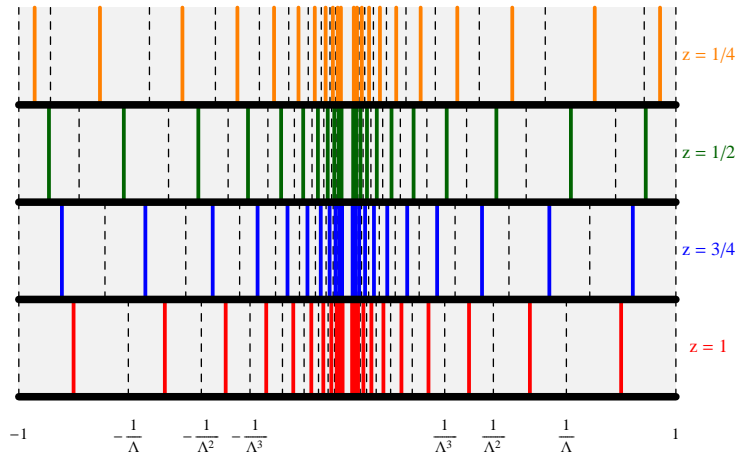


Figure 1.5: Yoshida's discretization scheme and the interleaved method.

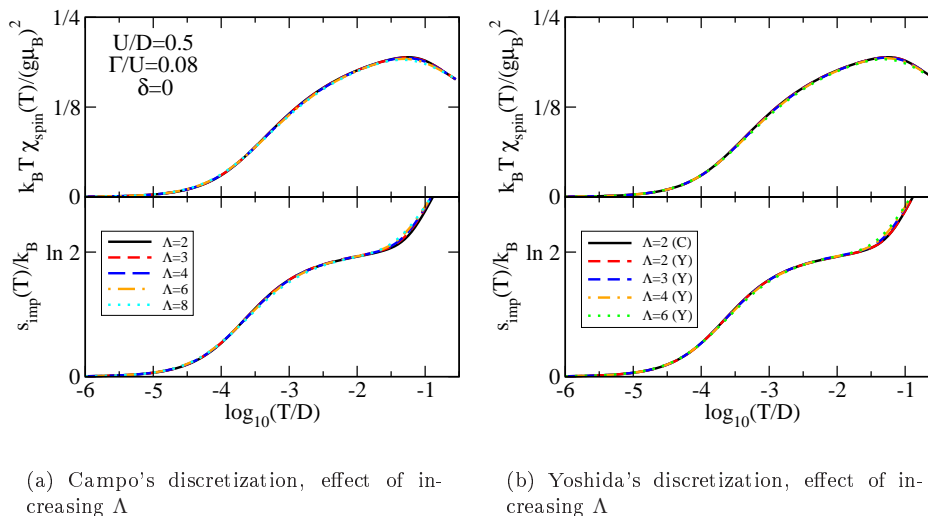
(a) Campo's discretization, effect of increasing  $\Lambda$ (b) Yoshida's discretization, effect of increasing  $\Lambda$ 

Figure 1.6: Comparison of magnetic susceptibility and entropy of the single-impurity Anderson model calculated using two different discretization types and for different values of the discretization parameter  $\Lambda$ . The coarse results were post-processed by averaging over  $z$  (the  $z$ -trick) and even-odd effects were removed by averaging over two consecutive NRG iteration steps.

very satisfactory results. Using the  $z$ -trick, the discretization parameter  $\Lambda$  can be increased to large values. In Fig. 1.6 we illustrate the rapid convergence to the  $\Lambda \rightarrow 1$  limit in the case of both improved methods. In the case of Yoshida discretization, the correction factor  $A_\Lambda$  was used, while no such correction is necessary in the case of Campo discretization.

Varying the sliding parameter  $z$  can also be used to assess numerical accuracy of the results by comparing eigenvalue spectra computed for different values of  $z$ . This is particularly important if the finite-size spectrum itself is the result of interest: the  $z$ -trick namely cannot be used to average the spectra in a meaningful manner. For large  $\Lambda$ , the spectra for different  $z$  can differ substantially, even though the  $z$ -averaged quantities (such as spectral functions) are an excellent approximation to the  $\Lambda \rightarrow 1$  results.

There is no good a priori recipe for choosing the value of  $\Lambda$ , the number of values of  $z$ , and the number of states retained in the NRG iteration; this depends on the number of impurities (i.e. the degeneracy), the values of model parameters and the quantities computed. For each new class of problems, a convergence study should be performed.

The density of states (DOS) in the conduction band is usually taken to be independent of energy, i.e.  $\rho = \text{const}$ , which is also known as the flat-band approximation. This choice is particularly convenient as it leads to analytic simplicity and some calculations can be performed in closed form.<sup>92</sup> In addition, RG treatment of the problem has shown that provided that all the energy scales of the problem are much smaller than the bandwidth, the form of the DOS at large energies is irrelevant in the RG sense.<sup>1</sup> Nevertheless, NRG calculations can be setup for an arbitrary DOS of the conduction electrons.<sup>39, 41, 89, 91, 93</sup> “NRG Ljubljana” has built-in support for flat bands (`band=flat`) and for tight-binding bands with cosine dispersion (`band=cosine`) where the hybridization function is  $\Gamma(\epsilon) \propto \sqrt{1 - (\epsilon/D)^2}$ . There is also a stub for arbitrary DOS/hybridization to be defined by the user (`band=dmft`), which is required if NRG is used as the impurity solver in DMFT.

### 1.3 Symmetries and basis construction

The efficiency of NRG calculations can be significantly improved if the symmetries of the problem are taken into consideration. In addition to the performance concerns, the implementation of symmetries is important on more fundamental ground: if the conservation laws are not built-in, numerical round-off errors tend to induce accidental symmetry breaking which, if relevant, can lead to erroneous results. Continuous symmetries (such as  $SU(2)_{\text{spin}}$ ,  $SU(2)_{\text{isospin}}$ ,  $U(1)_{\text{charge}}$ ) can be taken into account by constructing the basis states using the Lie group representation theory (i.e. Clebsch-Gordan coefficients and the Wigner-Eckart theorem).<sup>2</sup> Discrete symmetries (such as parity or particle-hole  $Z_2$  symmetries) can be taken into account by projecting basis states to invariant subspaces with well defined  $Z_2$  quantum number using suitable projection operators. By taking explicitly into account the full symmetry of the problem, we can make a formerly intractable problem within the reach of modern computers. For example, while not so long ago it was deemed difficult to obtain anything but the NRG eigenvalue flows for the two-channel problems,<sup>18</sup> it is now possible to perform calculations of thermodynamic and even dynamic properties of multi-impurity two-channel problems.<sup>32</sup> In the current implementation of “NRG Ljubljana”, the following symmetry types are supported:

- $U(1)_{\text{charge}} \times U(1)_{\text{spin}}$ , i.e. good quantum numbers are charge  $Q$  and spin projection  $S_z$  (symmetry type `QSZ` in “NRG Ljubljana”) – suitable for general quantum impurity models in the presence of the magnetic field;
- $U(1)_{\text{charge}} \times U(1)_{\text{spin}} \times Z_2$ , i.e. good quantum numbers are charge  $Q$ , spin projection  $S_z$  and parity  $P$  (symmetry type `QSZLR` in “NRG Ljubljana”) – suitable for models with reflection symmetry;
- $U(1)_{\text{charge}} \times SU(2)_{\text{spin}}$ , i.e. good quantum numbers are charge  $Q$  and total spin  $S$  (symmetry type `NRG`) – suitable for general QIMs in the absence of the magnetic field;
- $U(1)_{\text{charge}} \times SU(2)_{\text{spin}} \times Z_2$ , i.e. good quantum numbers are charge  $Q$ , total spin  $S$  and parity  $P$  (symmetry type `QSLR`);
- $SU(2)_{\text{iso}} \times SU(2)_{\text{spin}}$ , i.e. good quantum numbers are total isospin  $I$  and total spin  $S$  (symmetry type `ISO`) – suitable for QIMs at the particle-hole symmetric point;
- $SU(2)_{\text{iso}} \times SU(2)_{\text{spin}} \times Z_2$ , i.e. good quantum numbers are total isospin  $I$ , total spin  $S$  and parity  $P$  (symmetry type `ISOLR`).

		(q, s)	States (k)
(q, s)	States (k)	(-2, 0)	1
(-1, 0)	1	(-1, $\frac{1}{2}$ )	$b_{\uparrow}^{\dagger}, a_{\uparrow}^{\dagger}$
(0, $\frac{1}{2}$ )	$a_{\uparrow}^{\dagger}$	(0, 0)	$b_{\downarrow}^{\dagger}b_{\uparrow}^{\dagger}, \frac{1}{\sqrt{2}}(a_{\downarrow}^{\dagger}b_{\uparrow}^{\dagger} - a_{\uparrow}^{\dagger}b_{\downarrow}^{\dagger}), a_{\downarrow}^{\dagger}a_{\uparrow}^{\dagger}$
(1, 0)	$a_{\uparrow}^{\dagger}a_{\uparrow}^{\dagger}$	(0, 1)	$b_{\uparrow}^{\dagger}a_{\uparrow}^{\dagger}$
(a) One channel		(1, $\frac{1}{2}$ )	$a_{\uparrow}^{\dagger}b_{\downarrow}^{\dagger}b_{\uparrow}^{\dagger}, b_{\uparrow}^{\dagger}a_{\downarrow}^{\dagger}a_{\uparrow}^{\dagger}$
		(2, 0)	$a_{\uparrow}^{\dagger}a_{\downarrow}^{\dagger}b_{\uparrow}^{\dagger}b_{\downarrow}^{\dagger}$
		(b) Two channels	

Table 1.1: Basis states for additional sites for (Q,S) basis represented by the corresponding electron creation operators that need to be applied on the empty vacuum state. Bold small-case  $\mathbf{q}$  and  $\mathbf{s}$  are the quantum numbers of charge and spin on the added site(s), while  $\mathbf{k}$  indexes different states with the same (q, s).

For each symmetry type, the basis and coefficients for various NRG transformations are derived symbolically using a Mathematica program that uses the `sneg` library. In the following, we will describe the (Q, S) and (I, S) basis; other symmetry types are conceptually similar.

### 1.3.1 Construction of (Q, S) basis – symmetry type NRG

At the very least, all physically relevant models are charge-conserving. In the absence of the magnetic field, the problems are also rotationally invariant in the spin space; the total spin  $S$  and the component  $S_z$  are then also conserved. In addition, the component  $S_z$  can be eliminated from the problem by the use of the Wigner-Eckart theorem. It follows that we can classify states in subspaces according to quantum numbers  $Q$  and  $S$ .

We first consider the case of a single conduction channel. For brevity, we denote by  $a_{\mu}^{\dagger}$  the creation operator for an electron of spin  $\mu$  on the site of the Wilson chain that is added at the  $(N+1)$ th NRG iteration, i.e.  $a_{\mu}^{\dagger} = f_{N+1,\mu}^{\dagger}$ . The Fock space for the new site is composed of four states. Due to rotational invariance, states form spin-multiplets. A single state from each such multiplet needs to be retained, as all other members of the multiplet can be taken into account using the Wigner-Eckart theorem; by convention, in each multiplet with spin  $S$  we retain the state with the highest projection  $S_z = S$ . The four basis states for the additional site are thus represented by the three states given in Table 1.1a. In two-channel channel problems, two sites are added to the Wilson chain in each iteration, one from each conduction band. The creation operators for the second band are denoted by  $b_{\mu}^{\dagger} = f_{N+1,\mu,2}^{\dagger}$ . The 16 states that form the Fock space of the two newly added sites are represented by the 10 states given in Table 1.1b.

We also need a prescription for generating a basis with well defined  $Q$  and  $S$  for  $(N+1)$ -site Wilson chain given the eigenstates of the  $N$ -site Wilson chain from the previous iteration. This is easily accomplished using the angular momentum algebra (Clebsch-Gordan coefficients).<sup>1,2</sup> Let  $F_i(QS)$  denote the subspace  $\tilde{Q}\tilde{S}$  at stage  $N$  used to construct states  $|QSS_z r i\rangle_{N+1}$  with well defined  $Q, S, S_z$  at stage  $N+1$ ; index  $i$  numbers the possible ways of adding the angular momenta together ( $i = 1, \dots, 4$  for one-channel case,  $i = 1, \dots, 16$  for two-channel cases), while  $r$  numbers the consecutive eigenstates in the subspace  $\tilde{Q}\tilde{S}$  at step  $N$ . For convenience, we also define  $f_i^{\mu}(S_z) = \tilde{S}_z = S_z - \mu$ , the spin projection  $\tilde{S}_z$  for  $\mu$ -term in the expression, and  $g_i^{\mu}(SS_z) = \tilde{S}\tilde{S}_z$ . With this short-hand notation established, we are able to write the prescription as

$$|QSS_z r i\rangle_{N+1} = \sum_{\mu=-S(i)}^{S(i)} \langle g_i^{\mu}(SS_z); S(i), \mu | SS_z \rangle |F_i(QS)f_i^{\mu}(S_z)r\rangle_N \otimes |i, \mu\rangle, \quad (1.6)$$

$i$	$\tilde{Q}$	$\tilde{S}$	$(\mathbf{q}, \mathbf{s}, \mathbf{k})$
1	$Q + 2$	$S$	$(-2, 0, 1)$
2	$Q + 1$	$S - \frac{1}{2}$	$(-1, \frac{1}{2}, 1)$
3	$Q + 1$	$S + \frac{1}{2}$	$(-1, \frac{1}{2}, 1)$
4	$Q + 1$	$S - \frac{1}{2}$	$(-1, \frac{1}{2}, 2)$
5	$Q + 1$	$S + \frac{1}{2}$	$(-1, \frac{1}{2}, 2)$
6	$Q$	$S$	$(0, 0, 1)$
7	$Q$	$S$	$(0, 0, 2)$
8	$Q$	$S$	$(0, 0, 3)$
9	$Q$	$S - 1$	$(0, 1, 1)$
10	$Q$	$S$	$(0, 1, 1)$
11	$Q$	$S + 1$	$(0, 1, 1)$
12	$Q - 1$	$S - \frac{1}{2}$	$(1, \frac{1}{2}, 1)$
13	$Q - 1$	$S + \frac{1}{2}$	$(1, \frac{1}{2}, 1)$
14	$Q - 1$	$S - \frac{1}{2}$	$(1, \frac{1}{2}, 2)$
15	$Q - 1$	$S + \frac{1}{2}$	$(1, \frac{1}{2}, 2)$
16	$Q - 2$	$S$	$(2, 0, 1)$

(a) One channel

$i$	$\tilde{Q}$	$\tilde{S}$	$(\mathbf{q}, \mathbf{s}, \mathbf{k})$
1	$Q + 1$	$S$	$(-1, 0, 1)$
2	$Q$	$S - \frac{1}{2}$	$(0, \frac{1}{2}, 1)$
3	$Q$	$S + \frac{1}{2}$	$(0, \frac{1}{2}, 1)$
4	$Q - 1$	$S$	$(1, 0, 1)$

(b) Two channels

Table 1.2: Subspaces  $F_i(QS) = (\tilde{Q}, \tilde{S})$  and basis states for the additional site used to construct  $i$ th combination of basis states for the new iteration for  $(Q, S)$  basis

where  $\langle S_1 m_1; S_2 m_2 | S m \rangle$  denotes the Clebsch-Gordan coefficient for joining spins  $S_1$  and  $S_2$  into spin  $S$ ,  $|\rangle_{N+1}$  and  $|\rangle_N$  denote states for  $(N + 1)$ -site and  $N$ -site Wilson chain,  $|i, \mu\rangle$  are the states on the added site(s) tabulated in Table 1.1 and  $S(i) = \mathbf{s}$ , the total spin quantum number of the  $|i\mu\rangle$  state.

The rules for forming the new subspaces are given in Table 1.2. In “NRG Ljubljana”, these tables can be found in files `coef/1ch-In.cpp` and `coef/2ch-In.cpp` or, generally, in `coef/*-In.cpp`. As an example,  $i = 2$  and  $i = 3$  in the one-channel case correspond to two different ways of obtaining total spin  $S$  by adding a spin- $\frac{1}{2}$  object, either from  $\tilde{S} = S - \frac{1}{2}$  or from  $\tilde{S} = S + \frac{1}{2}$ . The relevant routines are `input_subspaces`, `nrg_make_subspaces_list`, and `nrg_makematrix`. It should be noted in passing that a singlet and a triplet never couple into a singlet state (that would be a violation of the triangle inequality). This must be taken into account when constructing state  $i = 10$  in the two-channel case;  $S = 0$  is then forbidden (such checks are performed by routine `newcombination_allowed`).

### 1.3.2 Construction of $(I, S)$ basis – symmetry type ISO

When the  $U(1)_{\text{charge}}$  conservation of charge symmetry can be extended to the full  $SU(2)_{\text{iso}}$  isospin symmetry, an additional complication arises due to the phase factor in the definition of the isospin down component of the tensor operator (which corresponds to the annihilation operator). The brackets of creation and annihilation operators must be expressed using the irreducible matrix elements

$$\langle I' I'_z S' S'_z r' | f_{i,\mu}^\dagger | I I_z S S_z r \rangle = \langle I I_z; \frac{1}{2} | I' I'_z \rangle \langle S S_z; \frac{1}{2} \mu | S' S'_z \rangle \langle I' S' r' | f_i | I S r \rangle \quad (1.7)$$

and

$$\langle I' I'_z S' S'_z r' | f_{i,\mu} | I I_z S S_z r \rangle = (-1)^i (-2\mu) \langle I I_z; \frac{1}{2}, -\frac{1}{2} | I' I'_z \rangle \langle S S_z; \frac{1}{2}, -\mu | S' S'_z \rangle \langle I' S' r' | f_i | I S r \rangle. \quad (1.8)$$

Here  $i$  is the site index which takes even or odd values on the underlying bipartite lattice. As the problem is assumed to be spin and isospin isotropic, neither  $S_z$  nor  $I_z$  play any role in the

		(i, s)	States (k)
(i, s)	States (k)	(1, 0)	$a_{\downarrow}^{\dagger} a_{\uparrow}^{\dagger} b_{\downarrow}^{\dagger} b_{\uparrow}^{\dagger}$
$(\frac{1}{2}, 0)$	$a_{\downarrow}^{\dagger} a_{\uparrow}^{\dagger}$	$(\frac{1}{2}, \frac{1}{2})$	$a_{\uparrow}^{\dagger} b_{\downarrow}^{\dagger} b_{\uparrow}^{\dagger}, a_{\downarrow}^{\dagger} a_{\uparrow}^{\dagger} b_{\uparrow}^{\dagger}$
$(0, \frac{1}{2})$	$a_{\uparrow}^{\dagger}$	(0, 1)	$-a_{\uparrow}^{\dagger} b_{\uparrow}^{\dagger}$
(a) One channel		(0, 0)	$-\frac{1}{\sqrt{2}} (a_{\downarrow}^{\dagger} a_{\uparrow}^{\dagger} + b_{\downarrow}^{\dagger} b_{\uparrow}^{\dagger}), \frac{1}{\sqrt{2}} (a_{\downarrow}^{\dagger} b_{\uparrow}^{\dagger} - a_{\uparrow}^{\dagger} b_{\downarrow}^{\dagger})$
		(b) Two channels	

Table 1.3: Basis states for additional site in the isospin-spin  $(I, S)$  basis. Bold small-case  $\mathbf{i}$  and  $\mathbf{s}$  are the quantum numbers of charge and spin on the added site(s), while  $\mathbf{k}$  indexes different states with the same  $(\mathbf{i}, \mathbf{s})$ .

diagonalization of  $H_{N+1}$ . The basis states for the added site of the Wilson chain are given in Table 1.3.

The invariant subspaces are constructed in analogy to the case of  $(Q, S)$  basis in previous subsection. Again  $F_i(IS)$  denotes the subspace  $\tilde{I}\tilde{S}$  at stage  $N$  used to construct states  $|II_zSS_zri\rangle_{N+1}$  at stage  $N+1$ . We also define  $f_i^{\alpha}(I_z) = \tilde{I}_z = I_z - \alpha$ ,  $f_i^{\mu}(S_z) = \tilde{S}_z = S_z - \mu$ ,  $g_i^{\alpha}(II_z) = \tilde{I}\tilde{I}_z$  and  $g_i^{\mu}(SS_z) = \tilde{S}\tilde{S}_z$ . The new basis is then formed using a double application of the angular momentum addition rules:

$$\begin{aligned}
|II_zSS_zi\rangle_{N+1} &= \sum_{\alpha=-I(i)}^{I(i)} \sum_{\mu=-S(i)}^{S(i)} \langle g_i^{\alpha}(II_z); I(i), \alpha | II_z \rangle \langle g_i^{\mu}(SS_z); S(i), \mu | SS_z \rangle \\
&\quad \times |F_i(IS) f_i^{\alpha}(I_z) f_i^{\mu}(S_z) r\rangle_N \otimes |i, \mu, \alpha\rangle.
\end{aligned} \tag{1.9}$$

$I(i)$  and  $S(i)$  correspond to  $\mathbf{i}$  and  $\mathbf{s}$  quantum numbers of states  $|i, \mu, \alpha\rangle$ . The rules for forming the states are summarized in Table 1.4.

$i$	$\tilde{I}$	$\tilde{S}$	$(\mathbf{i}, \mathbf{s}, \mathbf{k})$
1	$I - 1$	$S$	$(1, 0, 1)$
2	$I$	$S$	$(1, 0, 1)$
3	$I + 1$	$S$	$(1, 0, 1)$
4	$I - \frac{1}{2}$	$S - \frac{1}{2}$	$(\frac{1}{2}, \frac{1}{2}, 1)$
5	$I + \frac{1}{2}$	$S - \frac{1}{2}$	$(\frac{1}{2}, \frac{1}{2}, 1)$
6	$I - \frac{1}{2}$	$S + \frac{1}{2}$	$(\frac{1}{2}, \frac{1}{2}, 1)$
7	$I + \frac{1}{2}$	$S + \frac{1}{2}$	$(\frac{1}{2}, \frac{1}{2}, 1)$
8	$I - \frac{1}{2}$	$S - \frac{1}{2}$	$(\frac{1}{2}, \frac{1}{2}, 2)$
9	$I + \frac{1}{2}$	$S - \frac{1}{2}$	$(\frac{1}{2}, \frac{1}{2}, 2)$
10	$I - \frac{1}{2}$	$S + \frac{1}{2}$	$(\frac{1}{2}, \frac{1}{2}, 2)$
11	$I + \frac{1}{2}$	$S + \frac{1}{2}$	$(\frac{1}{2}, \frac{1}{2}, 2)$
12	$I$	$S - 1$	$(0, 1, 1)$
13	$I$	$S$	$(0, 1, 1)$
14	$I$	$S + 1$	$(0, 1, 1)$
15	$I$	$S$	$(0, 0, 1)$
16	$I$	$S$	$(0, 0, 2)$

(a) One channel

(b) Two channels

Table 1.4: Subspaces  $F_i(IS) = (\tilde{I}, \tilde{S})$  and basis states for the additional site used to construct  $i$ th combination of basis states for the new iteration in the  $(I, S)$  basis

## 1.4 RG transformation and iterative diagonalisation

In this section we describe how the hopping Hamiltonian is actually solved. We define a series of finite-size Hamiltonians of the form

$$H_N = \Lambda^{N/2} \left[ H_{\text{imp}} + H_C + \sum_{n=0}^N \sum_{\mu, \alpha} \Lambda^{-n/2} \xi_n (f_{n, \mu, \alpha}^\dagger f_{n+1, \mu, \alpha} + \text{H.c.}) \right], \quad (1.10)$$

so that the full Hamiltonian is given by the limit

$$H = \lim_{N \rightarrow \infty} \left( \Lambda^{-N/2} H_N \right). \quad (1.11)$$

The factor  $\Lambda^{N/2}$  in the definition of  $H_N$  rescales the energy scale so that the smallest dimensionless excitation energy of  $H_N$  becomes of order  $\mathcal{O}(1)$ . In some sense this is reminiscent of the rescaling of the fields in the momentum space renormalization or rescaling of the free energy per site in the block-spin renormalization. The NRG iteration is then defined by the recursion relation

$$H_{N+1} = R \{ H_N \} = \sqrt{\Lambda} H_N + \sum_{\mu, \alpha} \xi_N (f_{n, \mu, \alpha}^\dagger f_{n+1, \mu, \alpha} + \text{H.c.}). \quad (1.12)$$

The energies are rescaled by  $\sqrt{\Lambda}$  and one new site (one-channel problems) or two new sites (two-channel problems) from the Wilson chain are attached to the system, see Fig. 1.7. This recursion relation is the fundamental aspect of the NRG.<sup>1,2</sup> Due to even-odd effects, the RG transformation is actually defined by two consecutive NRG iterations:

$$H_{N+2} = R^2 \{ H_N \}, \quad (1.13)$$

so that the renormalization flow in the NRG is represented by the sequence of Hamiltonians

$$\dots \rightarrow H_{N-2} \rightarrow H_N \rightarrow H_{N+2} \rightarrow \dots \quad (1.14)$$

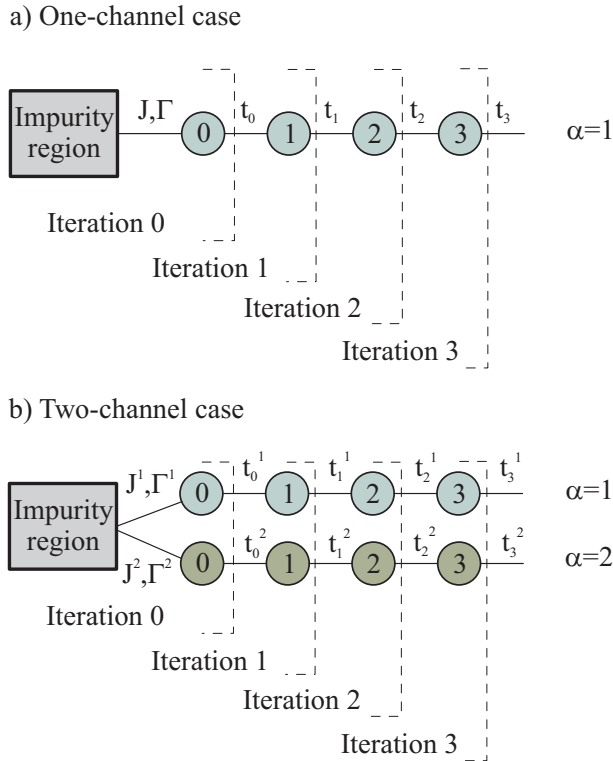


Figure 1.7: Hopping Hamiltonians and the successive iterations of the NRG procedure: one site from each channel is added during each RG step. As far as the NRG iteration is considered, the impurity region is a black box: all that is required are the eigenstates of the sum of the impurity and the coupling Hamiltonians,  $H_{\text{imp}} + H_C$ , and the irreducible matrix elements of the creation operators for an electron on the first (indexed as 0) site of the hopping Hamiltonian computed in the eigenbasis.

A simple way of seeing that  $R$  by itself cannot be an RG transformation is that during an iteration step the energy levels are rescaled by  $\sqrt{\Lambda}$ , therefore  $R$  cannot have a fixed point, since two successive energies in the discretized conduction-band Hamiltonian are separated by a factor of  $\Lambda$ .<sup>94</sup>  $R^2$ , however, does have fixed points.<sup>1</sup> It is also clear that the fixed point for even and odd  $N$  are generally different.<sup>1, 18</sup> The number of NRG steps performed is set by parameter  $N_{\text{max}}$ .

It should be noted in passing that the word “group” in renormalization group is actually inappropriate; in fact, it is in fact a “semi-group”. There is namely no inverse transformation. This is related to the fact that information is “lost” (integrated out), either by doing coarse graining (real-space RG) or by truncation (NRG). An inverse NRG iteration is therefore impossible.<sup>95</sup>

The Hamiltonian  $H_N$  describes the physics at the energy (temperature) scale

$$T_N \propto \frac{D}{k_B} \Lambda^{-N/2} / \bar{\beta} \quad (1.15)$$

or, equivalently, at the length scale

$$L_N \propto \bar{\beta} \Lambda^{N/2} / k_F. \quad (1.16)$$

Here  $\bar{\beta}$  is a parameter of order  $\mathcal{O}(1)$ ; the corresponding setting in “NRG Ljubljana” is **betabar**.

The exact definition of  $T_N$  depends on the discretization scheme:

$$\begin{aligned} T_N &= \frac{D}{k_B} \frac{1}{2} (1 + \Lambda^{-1}) \Lambda^{-(N-1)/2} / \bar{\beta}, & \text{for disc=wilson,} \\ T_N &= \frac{D}{k_B} \frac{1}{2} (1 + \Lambda^{-1}) \Lambda^{-(N-z)/2} / \bar{\beta}, & \text{for disc=yoshida,} \\ T_N &= \frac{D}{k_B} \frac{1 - \Lambda^{-1}}{\ln \Lambda} \Lambda^{-(N-z)/2} / \bar{\beta}, & \text{for disc=campo.} \end{aligned} \quad (1.17)$$

From Eqs. (1.15) and (1.16) it follows that NRG iteration corresponds to  $L \rightarrow \infty$  and  $T \rightarrow 0$  at the same time, but in a way that the size of the system is finite at all times. From this it follows that NRG gives *finite-size* spectra. It should be kept in mind that the ground state degeneracy of a finite-size spectrum is obtained by taking the limit  $T \rightarrow 0$  first, then  $L \rightarrow \infty$ . By taking first  $L \rightarrow \infty$  and then  $T \rightarrow 0$ , a different GS degeneracy can be obtained. The two limits do not commute<sup>96,97</sup>! One should be aware of this when comparing with results obtained by means of quantum-field-theoretical methods in the  $L \rightarrow \infty$  limit.

One might expect that due to the exponential decrease of hopping parameters it might be possible to treat the successive sites in the Wilson chain by perturbation theory. This is not the case:<sup>1</sup> when adding the  $(N + 1)$ st site(s) to a chain of  $N$  sites, the coupling of order  $\Lambda^{-N/2}$  is a strong perturbation for the lowest eigenstates of the  $N$ -site chain which are also on the energy scale of  $\Lambda^{-N/2}$ . We thus add a new site by performing an exact diagonalisation of a matrix  $H_{N+1}$ .

One NRG iteration (1.12) consists of using the states from previous step to construct the Hamiltonian  $H_{N+1}$  (`nrg_makematrix` routine), then diagonalizing it numerically (`diagonalize` routine). The full information about the system at step  $N$  is contained in the eigenstates of  $H_N$  and in the irreducible matrix elements  $\langle \|f_N\| \rangle$  (class `IterInfo`); this is clearly a much more detailed description compared to a small set of coupling parameters used in the conventional RG (scaling) approach. The Hamiltonian is written in the direct product basis  $|Q_S r i\rangle_{N+1} \sim |Q_S r\rangle \otimes i$  [here we consider the case of (Q,S) basis, see Sec. 1.3 for other cases], therefore the Hamiltonian matrix takes the form of a block-matrix: diagonal blocks are diagonal matrices, the diagonal elements being the rescaled eigenvalues of the states  $|Q_S r\rangle$  from the previous iteration; the out-of-diagonal blocks are constructed from the irreducible matrix elements  $\langle Q_S r \| f \| Q' S' r' \rangle$  weighted by coefficients that can be derived from the corresponding Clebsch-Gordan coefficients (see routine `nrg_makematrix`). These coefficients are given in Table 1.5 for the case of (Q,S) basis (see also Ref. 2). In “NRG Ljubljana”, these coefficients can be found in `coef/1ch-offdiag.cpp` and `coef/2ch-offdiag.cpp` or, generally, in `coef/*-offdiag.cpp`.

We then diagonalize the Hamiltonian in each invariant sector separately to obtain the eigenstates

$$|Q_S \omega\rangle = \sum_{ri} U_{QS}(\omega, ri) |Q_S r i\rangle, \quad (1.18)$$

where  $U_{QS}$  is the unitary matrix which brings each Hamiltonian matrix in its diagonal form. Before proceeding to the next NRG iteration, the irreducible matrix elements of the newly added site(s),  $\langle Q_S i \| f_{N+1, \mu\alpha}^\dagger \| Q' S' i' \rangle$ , need to be recomputed from the irreducible matrix elements  $\langle Q_S i \| f_{N, \mu\alpha}^\dagger \| Q' S' i' \rangle$  from the previous iteration. The coefficients are given in tables 1.6 and 1.7 and can be found in files `coef/1ch-spinupa.cpp`, `coef/1ch-spindowna.cpp`, `coef/2ch-spinupa.cpp`, `coef/2ch-spindowna.cpp`, `coef/2ch-spinupb.cpp`, `coef/2ch-spindownb.cpp` or, generally, in `coef/1ch-*.cpp`; the corresponding routines in “NRG Ljubljana” are `recalc_f` and `recalc_irreduc`.

Since the total number of states is an exponential function of the iteration number  $N$  ( $\propto 4^N$  in the one-channel case and  $\propto 16^N$  in the two-channel case), Wilson proposed to simply *truncate* the number of states to some manageable size of the order of 1000 after each NRG iteration. The idea is that, since the coupling between consecutive sites of the chain decreases exponentially for increasing chain length, only the lowest-lying eigenstates are renormalized and the separation of scales is thus maintained iteration by iteration.<sup>1,98</sup> This works because the matrix elements of  $f_N^\dagger$

$i$	$i'$	channel	coefficient
1	2	1	1
1	3	1	1
2	4	$-\frac{\sqrt{2S}}{\sqrt{1+2S}}$	
3	4	$\frac{\sqrt{2S+2}}{\sqrt{1+2S}}$	

(a) One channel

$i$	$i'$	channel	coefficient
1	2	b	1
1	3	b	1
1	4	a	1
1	5	a	1
2	6	b	$-\frac{\sqrt{2S}}{\sqrt{1+2S}}$
2	7	a	$-\frac{\sqrt{S}}{\sqrt{1+2S}}$
2	9	a	1
2	10	a	$\frac{\sqrt{1+S}}{\sqrt{1+2S}}$
3	6	b	$\frac{\sqrt{2(1+S)}}{\sqrt{1+2S}}$
3	7	a	$\frac{\sqrt{1+S}}{\sqrt{1+2S}}$
3	10	a	$\frac{\sqrt{S}}{\sqrt{1+2S}}$
3	11	a	1
4	7	b	$-\frac{\sqrt{S}}{\sqrt{1+2S}}$
4	8	a	$-\frac{\sqrt{2S}}{\sqrt{1+2S}}$
4	9	b	-1
4	10	b	$-\frac{\sqrt{1+S}}{\sqrt{1+2S}}$
5	7	b	$\frac{\sqrt{1+S}}{\sqrt{1+2S}}$
5	8	a	$\frac{\sqrt{2(1+S)}}{\sqrt{1+2S}}$
5	10	b	$-\frac{\sqrt{S}}{\sqrt{1+2S}}$
5	11	b	-1

(d) Two channels

$i$	$i'$	channel	coefficient
6	12	a	1
6	13	a	1
7	12	b	$-\frac{1}{\sqrt{2}}$
7	13	b	$-\frac{1}{\sqrt{2}}$
7	14	a	$-\frac{1}{\sqrt{2}}$
7	15	a	$-\frac{1}{\sqrt{2}}$
8	14	b	1
8	15	b	1
9	12	b	$\frac{\sqrt{-\frac{1}{2}+S}}{\sqrt{S}}$
9	14	a	$-\frac{\sqrt{-\frac{1}{2}+S}}{\sqrt{S}}$
10	12	b	$-\frac{\sqrt{\frac{S}{2}}}{\sqrt{S}}$
10	13	b	$\frac{\sqrt{\frac{S}{2}}}{\sqrt{S}}$
10	14	a	$\frac{\sqrt{1+S}}{\sqrt{S}}$
10	15	a	$-\frac{\sqrt{\frac{S}{2}}}{\sqrt{1+S}}$
11	13	b	$-\frac{\sqrt{\frac{3}{2}+S}}{\sqrt{1+S}}$
11	15	a	$\frac{\sqrt{\frac{3}{2}+S}}{\sqrt{1+S}}$
12	16	a	$-\frac{\sqrt{2S}}{\sqrt{1+2S}}$
13	16	a	$\frac{\sqrt{2(1+S)}}{\sqrt{1+2S}}$
14	16	b	$-\frac{\sqrt{2S}}{\sqrt{1+2S}}$
15	16	b	$\frac{\sqrt{2(1+S)}}{\sqrt{1+2S}}$

Table 1.5: Coefficients for off-diagonal blocks in the Hamiltonian matrix in the  $(Q, S)$  basis

$i$	$i'$	coefficient	$i$	$i'$	coefficient
2	1	1	3	1	1
4	3	$-\frac{\sqrt{2S'+1}}{\sqrt{S'+1}}$	4	2	$\frac{\sqrt{2S'+1}}{\sqrt{S'}}$

(a)  $Q' = Q - 1,$   
 $S' = S - \frac{1}{2}$

(b)  $Q' = Q - 1,$   
 $S' = S + \frac{1}{2}$

Table 1.6: Irreducible matrix elements  $\langle QSi || a^\dagger || Q'S'i' \rangle$  for creation operator on the additional site in one-channel problems

$i$	$i'$	coefficient	$i$	$i'$	coefficient	$i$	$i'$	coefficient	$i$	$i'$	coefficient
5	1	1	4	1	1	3	1	1	2	1	1
7	2	$\frac{\sqrt{2S'+1}}{2\sqrt{S'}}$	7	3	$-\frac{\sqrt{2S'+1}}{2\sqrt{S'+1}}$	6	2	$\frac{\sqrt{S'+\frac{1}{2}}}{\sqrt{S'}}$	6	3	$-\frac{\sqrt{S'+\frac{1}{2}}}{\sqrt{S'+1}}$
8	4	$\frac{\sqrt{S'+\frac{1}{2}}}{\sqrt{S'}}$	8	5	$-\frac{\sqrt{S'+\frac{1}{2}}}{\sqrt{S'+1}}$	7	4	$\frac{\sqrt{2S'+1}}{2\sqrt{S'}}$	7	5	$-\frac{\sqrt{2S'+1}}{2\sqrt{S'+1}}$
10	2	$-\frac{\sqrt{2S'-1}}{2\sqrt{S'}}$	9	2	-1	10	4	$\frac{\sqrt{2S'-1}}{2\sqrt{S'}}$	9	4	1
11	3	-1	10	3	$-\frac{\sqrt{2S'+3}}{2\sqrt{S'+1}}$	11	5	1	10	5	$\frac{\sqrt{2S'+3}}{2\sqrt{S'+1}}$
13	6	1	12	6	1	12	9	$\frac{\sqrt{S'+\frac{1}{2}}}{\sqrt{S'}}$	12	7	$-\frac{1}{\sqrt{2}}$
14	9	$-\frac{\sqrt{S'+\frac{1}{2}}}{\sqrt{S'}}$	14	7	$-\frac{1}{\sqrt{2}}$	13	7	$-\frac{1}{\sqrt{2}}$	12	10	$-\frac{\sqrt{S'}}{\sqrt{2}\sqrt{S'+1}}$
15	7	$-\frac{1}{\sqrt{2}}$	14	10	$\frac{\sqrt{S'}}{\sqrt{2}\sqrt{S'+1}}$	13	10	$\frac{\sqrt{S'+1}}{\sqrt{2}\sqrt{S'}}$	13	11	$-\frac{\sqrt{S'+\frac{1}{2}}}{\sqrt{S'+1}}$
15	10	$-\frac{\sqrt{S'+1}}{\sqrt{2}\sqrt{S'}}$	15	11	$\frac{\sqrt{S'+\frac{1}{2}}}{\sqrt{S'+1}}$	15	8	1	14	8	1
16	12	$\frac{\sqrt{S'+\frac{1}{2}}}{\sqrt{S'}}$	16	13	$-\frac{\sqrt{S'+\frac{1}{2}}}{\sqrt{S'+1}}$	16	14	$\frac{\sqrt{S'+\frac{1}{2}}}{\sqrt{S'}}$	16	15	$-\frac{\sqrt{S'+\frac{1}{2}}}{\sqrt{S'+1}}$

(a)  $Q' = Q-1, S' = S + \frac{1}{2}$       (b)  $Q' = Q-1, S' = S - \frac{1}{2}$       (c)  $Q' = Q-1, S' = S + \frac{1}{2}$       (d)  $Q' = Q-1, S' = S - \frac{1}{2}$

Table 1.7: Irreducible matrix elements  $\langle QSi || a^\dagger || Q'S'i' \rangle$  for creation operator  $a^\dagger$  (subtables a and b) and for creation operator  $b^\dagger$  (subtables c and d) on the additional site in two-channel problems

are largest for similar eigenstates of  $H_N$ , while the matrix elements of  $f_N^\dagger$  between the low-lying eigenstates of  $H_N$  and the highly excited states that are truncated are small.<sup>1</sup>

In “NRG Ljubljana”, truncation is controlled by parameters `keep`, `keepmin` and `keepenergy`. Parameter `keep` restrains the maximum number of eigenstates that may be kept at each iteration; it should be increased as much as possible within the limits set by available computational resources. If parameter `keepenergy` is set to a positive value, the energy cut-off truncation scheme is used: only the eigenstates with the (rescaled) energy below the value of the parameter will be retained. The use of the energy cut-off truncation is recommended since a high number of states is kept when the degeneracy is high, and a low number when the degeneracy is low; in this fashion, the computational time is divided optimally between the iterations. Finally, `keepmin` sets the minimum number of states to be kept. It should also be remarked that eigenstates in NRG tend to be clustered. If the states are truncated in the middle of such a cluster, systematic errors and symmetry breaking may be induced. Parameter `safeguard` enforces retention of additional states, so that the “gap” between the highest retained and the lowest discarded state is at least `safeguard`.

## 1.5 Computable quantities

While K. G. Wilson originally applied NRG to obtain the spectrum of excitations and the impurity contribution to the magnetic susceptibility,<sup>1</sup> methods to calculate other quantities were soon introduced: one can determine specific heat,<sup>99,100</sup> charge susceptibility,<sup>101</sup> entropy,<sup>90</sup> spin relaxation rates,<sup>102</sup> and various zero-frequency response functions and equal-time correlation functions.<sup>103</sup> NRG is demonstrably the most versatile tool in the field of quantum impurity physics.

### 1.5.1 Finite-size spectra and fixed points

The most easily obtained result in NRG is the spectrum of excitations above the ground state as a function of the temperature. An important amount of information may be extracted from the consideration of such spectra alone. It should be noted that the system size in NRG is finite

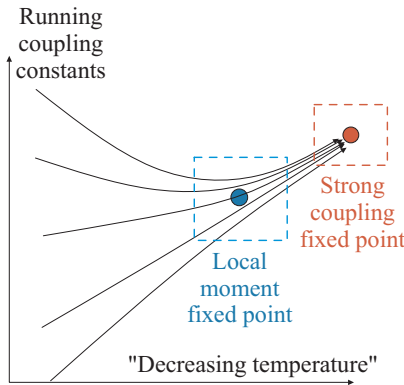


Figure 1.8: Schematic representation of the NRG renormalization flow. The horizontal direction represents the direction of decreasing energy scale (temperature), while the vertical direction represents the multi-dimensional space of the effective Hamiltonians (which can be considered to be parameterized by some large set of coupling constants). When the system is near a fixed point (dashed boxes), its properties can be described by a perturbative expansion around the fixed-point Hamiltonian. The diagram also illustrates the idea of universality: even for widely different microscopic Hamiltonians, the low-temperature behavior of the systems is essentially the same.

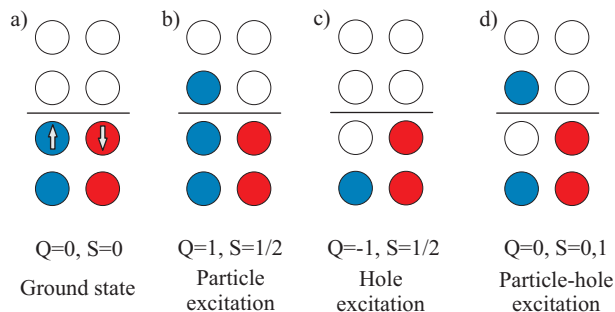


Figure 1.9: Pictorial representation of the ground state and excitations of a Fermi liquid.

at any iteration step: we say that we obtain *finite-size spectrum*. In contradistinction, the high-energy cutoff scaling methods such as Anderson's poor man's scaling,<sup>104</sup> multiplicative RG<sup>105</sup> and Yuval-Anderson's RG<sup>6</sup> work in the continuum limit ( $L \rightarrow \infty$ , where  $L$  is the system size).<sup>106</sup> Some important quantities, such as the ground state entropy, depend on whether the system size is finite or not when the  $T \rightarrow 0$  limit is taken<sup>96</sup> (see also Sec. 1.4).

If the lowest lying eigenstates for successive ( $N \rightarrow N + 2$ ) NRG transformations remain (nearly) unchanged, we say that a *fixed point* has been reached. More accurately, fixed-point Hamiltonian  $H^*$  is defined as

$$H^* = R^2\{H^*\}. \quad (1.19)$$

With NRG, one can study the various fixed points of a given QIM, deviations from the universal spectra (determined by the operator content of the fixed point<sup>106</sup>), and the cross-overs between the different fixed points, Fig. 1.8.

If the excitation spectrum of a fixed point is in a one-to-one relation to the excitations of free electron gas, such fixed point is called *Fermi liquid fixed point*. The spectra of Fermi liquid fixed points are composed of excitations that change particle number (particle and hole excitations) and excitations where a particle is promoted to a higher level (particle-hole excitations), and combinations thereof, Fig. 1.9. The excitations of non-Fermi liquid fixed points do not have such simple interpretation.

For Hamiltonian  $H_N$  near a fixed point  $H^*$ , the NRG recursion relation can be expanded in powers

of the deviation from the fixed point and linearized.<sup>1,2</sup> Defining  $\delta H_N = H_N - H^*$ , we write

$$\delta H_{N+2} = R^2\{H^* + \delta H_N\} - H^* \approx \mathcal{L}^* \delta H_N, \quad (1.20)$$

where  $\mathcal{L}^*$  is a linear transformation. Like any linear operator,  $\mathcal{L}^*$  can be diagonalized

$$\mathcal{L}^* O_l^* = \lambda_l^* O_l^*, \quad (1.21)$$

and we expand  $\delta H_N$  as

$$\delta H_N = \sum_l C_l \lambda_l^{*N/2} O_l^*. \quad (1.22)$$

For  $\lambda_l^* > 1$ , the contribution of corresponding eigenoperator  $O_l^*$  will grow with  $N$ : we say that such operators are *relevant*. For  $\lambda_l^* < 1$ , the contribution will vanish and we name such operators *irrelevant*. Finally, if  $\lambda_l^* = 1$ , the operator  $O_l^*$  is called *marginal* and its effect must be studied more carefully by considering non-linear corrections to the RG transformation.<sup>107</sup> The operator content of a fixed point determines its stability with respect to perturbations:<sup>2</sup> a fixed point with relevant operators is called *unstable*, while a fixed point with only irrelevant operators is *stable*. Fixed point with marginal operators can be either stable or unstable, or may lead to the emergence of lines of fixed point and to the breakdown of the universality.<sup>107</sup> The knowledge of the leading eigenoperators (i.e. those with the highest eigenvalues  $\lambda_l^*$ ) is instrumental in establishing *effective Hamiltonians* given by the fixed point Hamiltonian  $H^*$  plus correction terms:<sup>2</sup>

$$H_N^{\text{eff}} = H^* + \omega_1 \Lambda^{(N-1)/2} \delta H_1 + \omega_2 \Lambda^{(N-1)/2} \delta H_2 + \dots \quad (1.23)$$

where  $\omega_1$  and  $\omega_2$  are some coefficients which can be determined by analyzing the NRG spectrum. For example, corrections to the Fermi-liquid  $T = 0$  behavior of the Kondo model are determined by the leading irrelevant operators.<sup>1</sup>

Saving of eigenvalue results in “NRG Ljubljana” is controlled by parameters `trace`, `dumpenergies` and `dumpannotated`.

## 1.5.2 Static thermodynamic quantities: susceptibilities, entropy, heat capacity

Static thermodynamic quantities, such as magnetic susceptibility, heat capacity and entropy, are determined primarily by the energy level splittings of order  $k_B T$ . Energies much higher than  $k_B T$  above the ground state are exponentially suppressed, while excitations with much lower energy can be considered thermally washed out; this turns out to be a good approximation. Thermodynamic quantities at temperature  $T_N$  can thus be calculated from the energy spectrum at the  $N$ th stage of the NRG iteration.<sup>1,2,4</sup> In the following, brackets denote grand-canonical averaging

$$\langle O \rangle = \text{Tr}(O \exp(-\beta H)) / Z, \quad (1.24)$$

where  $Z$  is the partition function  $Z = \text{Tr}(e^{-\beta H})$  and  $\beta = 1/k_B T$ . In practice, the traces are computed in the truncated basis of NRG eigenstates at a given iteration step  $N$ , i.e. from a finite-size spectrum. In “NRG Ljubljana”, the temperature dependence of static thermodynamic quantities is output to file `chi` which must be postprocessed to obtain presentable results.

### Magnetic and charge susceptibility

The temperature-dependent impurity contribution to the magnetic susceptibility  $\chi_{\text{imp}}(T)$  is defined as

$$\chi_{\text{imp}}(T) = \frac{(g\mu_B)^2}{k_B T} (\langle S_z^2 \rangle - \langle S_z \rangle_0^2) \quad (1.25)$$

where  $S_z$  is the total spin and the subscript 0 refers to the situation when no impurities are present (i.e.  $H$  is simply the band Hamiltonian  $H_{\text{band}}$ ),  $g$  is the electronic gyromagnetic factor,

$\mu_B$  the Bohr magneton and  $k_B$  the Boltzmann's constant. It should be noted that the combination  $T\chi_{\text{imp}}/(g\mu_B)^2$  can be considered as an effective moment of the impurities,  $\mu_{\text{eff}}$ . In the presence of the magnetic field applied only to the impurity site,  $\langle S_z^2 \rangle$  needs to be replaced by  $\langle S_z^2 \rangle - \langle S_z \rangle^2$  in accordance to the fluctuation-dissipation theorem. It may also be remarked that while K. G. Wilson originally proposed to calculate  $\langle S_z^2 \rangle_0$  analytically, I find that it is more practical to actually perform a NRG calculation of  $S_z^2$  for a problem without impurities. This has an added benefit in that similar artefacts appear in  $\langle S_z^2 \rangle$  and  $\langle S_z^2 \rangle_0$  and they cancel when subtraction is performed.

By analogy, charge susceptibility is defined as

$$\chi_{\text{charge}}(T) = \frac{1}{k_B T} (\langle I_z^2 \rangle - \langle I_z \rangle_0^2), \quad (1.26)$$

where  $I_z$  is the total isospin (recall that  $I_z = Q/2$ ). In the absence of the particle-hole symmetry,  $\langle I_z^2 \rangle$  needs to be replaced by  $\langle I_z^2 \rangle - \langle I_z \rangle^2$ .

### Heat capacity and entropy

Defining energy as  $E = \langle H \rangle = \text{Tr}(H e^{-\beta H})$ , the heat capacity can be calculated from energy fluctuations as

$$C(T) = \frac{\partial E}{\partial T} = k_B \beta^2 [\langle H^2 \rangle - \langle H \rangle^2], \quad (1.27)$$

and we may define the impurity contribution to the heat capacity as  $C_{\text{imp}}(T) = C(T) - C_0(T)$ , where  $C_0$  is the heat capacity of the conduction band without impurities. Furthermore, we have  $\beta F = -\ln Z$  and  $E = F + TS$ , therefore

$$\frac{S}{k_B} = \frac{E - F}{k_B T} = \beta E - \beta F = \beta E + \ln Z, \quad (1.28)$$

and we may define the temperature-dependent impurity contribution to the entropy as  $S_{\text{imp}}(T) = S(T) - S_0(T)$ . From the quantity  $S_{\text{imp}}/k_B$  we can deduce the effective degrees-of-freedom  $\nu$  of the impurity as  $S_{\text{imp}}/k_B \sim \ln \nu$ .

The convergence with the number of states retained in the NRG iteration depends on the quantity being computed. For example, the energy accuracy required for a specific-heat calculation is considerably higher than that for the susceptibility.<sup>99</sup>

### 1.5.3 Correlation functions

To characterize the state of a quantum impurity system it is often useful to calculate various correlations functions, i.e. thermodynamic expectation values of operators such as the on-site occupancy  $\langle n_i \rangle$ , local charge-fluctuations  $\langle (\delta n)^2 \rangle = \langle (n_i - \langle n_i \rangle)^2 \rangle = \langle n_i^2 \rangle - \langle n_i \rangle^2$ , local-spin  $\langle \mathbf{S}_i^2 \rangle$  and spin-spin correlations  $\langle \mathbf{S}_i \cdot \mathbf{S}_j \rangle$ . In turn, these can be used to compute more complex quantities such as the concurrence which measures the entanglement between two qubits.<sup>108</sup>

In “NRG Ljubljana”, the operators of interest are specified by writing the corresponding expression in terms of the second quantization operators. A number of auxiliary routines are available to simplify this process and the most commonly occurring operators are already built in the program (configuration setting `ops`). During the problem setup step, the operators are transformed in their matrix forms and rotated into the eigenbasis of the initial Hamiltonian by performing suitable unitary transformations: all these steps are performed automatically “behind the scenes” by the Mathematica part of the NRG package. This approach turned out to be extremely flexible, since the user can focus on physics rather than hand-code low-level routines and worry about implementational details.

To be able to make full use of the symmetries of the problem, the operators need to be expressed in the form that makes them singlets with respect to the symmetry group. For example,  $n_i^2$  is

a spin-singlet, and can be directly computed in the  $(Q, S)$  basis. It is not, however, an iso-spin singlet, but  $(n_i - 1)^2 = q_i^2$  is. For a computation in the  $(I, S)$  basis, one therefore performs a calculation for  $q_i^2$  and adds  $2\langle n_i \rangle - 1 = 1$  to the results (recall that  $\langle n_i \rangle = 1$  due to the p-h symmetry). In the presence of mirror  $Z_2$  symmetry, it must be taken into account that operators may be even or odd with respect to the reflection. In the case of two impurities embedded in a series between two conduction leads, for example,  $n_e = n_1 + n_2$  is even, while  $n_o = n_1 - n_2$  is odd. In a calculation where reflection symmetry is explicitly taken into account, the expectation values  $\langle n_1 \rangle$  and  $\langle n_2 \rangle$  can be obtained by calculating suitable combinations of  $\langle n_e \rangle$  and  $\langle n_o \rangle$  after the NRG run.

More generally, “NRG Ljubljana” supports operators that are singlet, doublet or triplet with respect to spin and singlet or doublet with respect to isospin. This is sufficient for all calculations of interest, but support for more general symmetries may in principle be easily added.

### 1.5.4 Dynamic quantities

A major extension of the NRG was a method to calculate dynamic properties such as the spectral functions.<sup>20, 89, 109–112</sup> While  $T = 0$  conductance of Fermi-liquid systems may be obtained from finite-size spectra alone,  $T \neq 0$  and AC conductance, as well as the conductance of non-Fermi-liquid systems can only be computed if spectral functions are known.<sup>94, 113–117</sup> Using NRG, one can determine local single-particle (spectral function,  $\langle\langle d_\mu; d_\mu^\dagger \rangle\rangle_\omega$ ), magnetic (dynamic spin susceptibility,  $\langle\langle S_z; S_z \rangle\rangle_\omega$ ) and charge excitations (dynamic charge susceptibility,  $\langle\langle n; n \rangle\rangle_\omega$ ). It is also possible to distinguish between elastic and inelastic contributions to the scattering cross-section.<sup>118</sup>

The conventional approach to the NRG spectral density calculations is based on the observation of Sakai et al.<sup>20</sup> that as we proceed from one iteration to the next, the lowest few eigenstates split due to the interaction with the added shell states, while the intermediate lower levels do not show any essential change. The intermediate states thus form a good approximation of the eigenstates of the Hamiltonian in the  $N \rightarrow \infty$  limit and are thus used to compute the excitation energies and the transition matrices.

The spectral function matrix for multi-impurity problems is defined as

$$A_{ij} = -1/(2\pi)\text{Im}(G_{ij}^r + G_{ji}^r), \quad (1.29)$$

where  $G_{ij}^r(\omega) = \langle\langle d_{i\mu}; d_{j\mu}^\dagger \rangle\rangle_\omega$  is the (out-of-diagonal for  $i \neq j$ ) retarded Green’s function of the impurity. It can be computed using standard NRG techniques from matrix elements of the creation operators using the following spectral decompositions:

$$\begin{aligned} A_{i,j}(\omega > 0) &= \frac{1}{Z} \sum_{m, n_0} \text{Re} \left[ \left( \langle m | d_i^\dagger | n_0 \rangle \right)^* \langle m | d_j^\dagger | n_0 \rangle \right] \\ &\quad \times \delta(\omega - E_m), \\ A_{i,j}(\omega < 0) &= \frac{1}{Z} \sum_{m_0, n} \text{Re} \left[ \left( \langle m_0 | d_i^\dagger | n \rangle \right)^* \langle m_0 | d_j^\dagger | n \rangle \right] \\ &\quad \times \delta(\omega + E_n), \end{aligned} \quad (1.30)$$

where  $Z$  is the spectral sum  $Z = \text{Tr}(e^{-\beta H})$ , indices  $m_0, n_0$  with subscript 0 run over (eventually degenerate) ground states and indices  $m, n$  without a subscript over all states. Note that there is a sum rule

$$\int_{-\infty}^{\infty} A_{ij}(\omega) d\omega = \delta_{ij}, \quad (1.31)$$

which follows from the fermionic anti-commutation relation  $a_{i\mu}^\dagger a_{j\mu} + a_{j\mu} a_{i\mu}^\dagger = \delta_{ij}$ .

Calculations can be improved by directly calculating the one-particle self-energy  $\Sigma(\omega)$ ;<sup>98</sup> this approach leads to more accurate results and it is especially suitable for applications of NRG as an

impurity solver in the DMFT.<sup>79</sup> Further improvements include a better approach to merge partial spectral information from consecutive NRG iterations<sup>119</sup> (in “NRG Ljubljana” the result of the conventional spectrum calculation is output to files `spec*_pts_*.dat`, while the result obtained with the  $N/N+2$  trick is output to files `spec*_dens_*.dat`). For problems where the high-energy spectral features depend on the low-energy behavior of the system, the spectral density has to be computed taking into account the reduced density matrix obtained from the density matrix of the low-temperature fixed-point: this is the density-matrix NRG (DMNRG) developed by W. Hofstetter.<sup>120</sup> This approach is needed, for example, in the case of the Anderson impurity in magnetic field,<sup>120</sup> or for the side-coupled double quantum dot near the points of ground state level crossing.<sup>66</sup>

Recently, a time-dependent NRG was introduced<sup>121</sup> by generalizing the idea behind the DMNRG: time-dependent NRG makes possible to study the effects of sudden changes of the parameters and the ensuing relaxation to the steady state solution. In this approach, a density matrix in full Fock space is introduced by judiciously using the information from the discarded part of the NRG eigenstates. This idea has led to new approach for calculation of equilibrium spectral functions: the “full density matrix” NRG<sup>122</sup> or “complete Fock space” NRG.<sup>123</sup> This method does not suffer from over-counting of excitations, it fulfills sum rules and correctly reproduces spectral features at energies below the temperature.

An important observation for practical calculations is that as the number of states retained is increased, the calculated spectra do not suddenly change; they rather gradually improve and converge toward the true spectrum.<sup>20</sup> This implies that even rough spectra are qualitatively correct.

### 1.5.5 Spectrum broadening and smoothing

Since quantum impurity models are represented in NRG by a hopping Hamiltonian of a finite size, the computed spectral functions are represented as a sum of delta peaks. To obtain a meaningful continuous function, these peaks need to be broadened. The original approach to obtaining a smooth curve was by Gaussian broadening, followed by separate spline interpolation of results in odd and even steps, and by the averaging of the two curves.<sup>20</sup> A better approach is the logarithmic-exponential broadening:<sup>119</sup> each data point (delta function peak at  $\omega_0$ ) is smoothed into

$$F_b(\omega, \omega_0) = \frac{e^{-b^2/4}}{b\sqrt{\pi}} \exp\left(-\frac{(\ln\omega - \ln\omega_0)^2}{b^2}\right), \quad (1.32)$$

i.e. a Gaussian function on a logarithmic scale, where  $b$  is a broadening parameter, typically  $b = 0.3$ . One should keep in mind an important feature regarding the broadening procedure. Namely, due to broadening the spectral resolution at energy  $\omega$  is always limited to

$$\begin{aligned} \delta\omega_+ &= \omega \left( e^{b\sqrt{\ln 2}} - 1 \right) \\ \delta\omega_- &= \omega \left( 1 - e^{-b\sqrt{\ln 2}} \right) \end{aligned} \quad (1.33)$$

For high-energy part of the spectrum (say  $\omega = 1$ ) this limits the resolution to  $[-0.22; 0.28]$  at  $b = 0.3$ . Peaks sharper than this will thus appear broader than they truly are. NRG is therefore not a reliable method to determine the spectral features at high energies.

Furthermore, low energy features are also slightly deformed. The action of the broadening is to replace

$$f(\omega) = \int d\omega_0 f(\omega_0) \delta(\omega - \omega_0) \quad \rightarrow \quad \tilde{f}(\omega) = \int d\omega_0 f(\omega_0) F_b(\omega, \omega_0). \quad (1.34)$$

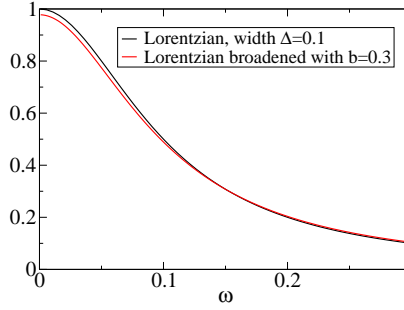


Figure 1.10: Effect of logarithmic broadening on a Lorentzian curve.

Let us consider its effect on a narrow Lorentzian of width  $\Delta$  centered at  $\omega = 0$ :

$$\begin{aligned} \tilde{f}(\omega) &= \int_0^\infty d\omega_0 \frac{\Delta^2}{\omega_0^2 + \Delta^2} F_b(\omega, \omega_0) \\ &= \int_{-\infty}^{+\infty} dy_0 \frac{\Delta^2}{\exp(2y_0) + \Delta^2} \frac{e^{-b^2/4}}{b\sqrt{\pi}} \exp\left(-\frac{(y - y_0)^2}{b^2}\right), \end{aligned} \quad (1.35)$$

where we performed substitution  $\ln \omega_0 = y_0$  and introduced  $y = \ln \omega$ . The limit  $\omega \rightarrow 0$  corresponds to  $y \rightarrow -\infty$ . The integrand is a Gaussian-like function centered at  $y$  with a  $y_0$  dependent weight  $\propto 1/(\exp(y_0^2) + \Delta^2)$ . For small enough  $\omega$  (to be concrete,  $\omega \ll \Delta$ ), this weight becomes a constant and the integral can be evaluated exactly. We find  $\lim_{\omega \rightarrow 0} \tilde{f}(\omega) = \exp(-b^2/4)$ . For  $b = 0.3$ , this gives 0.98. In other words, even in the absence of any other approximations, the logarithmic broadening at  $b = 0.3$  introduces an error of few percent in the Kondo peak weight. In addition, the Lorentzian is narrowed, see Fig. 1.10. These facts must be taken into account when quantitative details in the results are important. In that case  $b$  should be reduced as much as possible. Typically, the value of  $b$  is chosen to be 0.3 or less (parameter `loggauss_b`).

## 1.6 Recursion relations for operators

After each iteration, expectation values of operators of interest are computed and the irreducible matrix elements of these operators recomputed in the new eigenbasis for the next iteration. It is important to note that it is only possible to consider operators that transform as tensor operators with respect to the symmetry group that is taken into account in the NRG implementation. As an illustration, we consider the case of the (Q,S) symmetry and a tensor operator operator  $\hat{O}$  of rang  $M$  with respect to the spin SU(2) group. The information about the operator  $\hat{O}$  at iteration  $N$  is entirely contained in a matrix  $O_N$  of irreducible matrix elements  $\langle Q S r \| \hat{O} \| Q' S' r' \rangle$ . The non-zero subspaces for singlet operators have  $Q = Q'$  and  $S = S'$ , for doublet (creation) operators we must have  $Q = Q' + 1$  and  $S = S' \pm 1/2$  and for triplet operators (such as spin) we must have  $Q = Q'$  and  $S = S'$  or  $S = S' \pm 1$ . In the basis of eigenvalues  $|Q S \omega\rangle$  of the  $(N + 1)$ st iteration, we write

$$\langle Q S \omega \| \hat{O} \| Q' S' \omega' \rangle_{N+1} = \frac{\langle Q S S_z \omega | \hat{O}_\mu | Q' S' S'_z \omega' \rangle_{N+1}}{\langle S' S'_z; M \mu | S S_z \rangle} \quad (1.36)$$

To make this expression meaningful, we can choose, for example,  $S_z = S$ ,  $\mu = M$ ,  $S'_z = S - M$ . We then have

$$\langle Q S \omega \| \hat{O} \| Q' S' \omega' \rangle_{N+1} = \frac{\sum_{r' i' i} U_{QS}(\omega, r i) U_{Q' S'}(\omega', r' i') \langle Q S S r i | \hat{O}_M | Q' S', S - M, r' i' \rangle_{N+1}}{\langle S', S - M; M M | S S \rangle} \quad (1.37)$$

We then take into account the definitions of  $|QSS_zri\rangle$  states, (1.6), and write

$$\begin{aligned} \dots &= \sum_{ri,r'i'} \sum_{\alpha\beta} \frac{c(QS, Q'S', ii', \alpha\beta)}{\langle S', S-M; MM|SS\rangle} \\ &\times U_{QS}(\omega, ri) U_{Q'S'}(\omega', r'i') \langle F_i(QS) f_i^\alpha(S) r | \hat{O}_M | F_{i'}(Q'S') f_{i'}^\beta(S-M) r' \rangle_{N+1}, \end{aligned} \quad (1.38)$$

where  $c(QS, Q'S', ii', \alpha\beta)$  is a scalar product between  $(\mathbf{q}, \mathbf{s}, \mathbf{k})$  states on the added sites of the Wilson chain and  $\alpha, \beta$  are the corresponding  $s_z$  components of these states. We rewrite this as

$$\begin{aligned} \dots &= \sum_{ii', \alpha\beta} \frac{c(QS, Q'S', ii', \alpha\beta) \langle g_{i'}^\beta(S', S-M); MM | g_i^\alpha(SS) \rangle}{\langle S', S-M; MM|SS\rangle} \\ &\times \sum_{rr'} U_{QS}(\omega, ri) U_{Q'S'}(\omega', r'i') \langle F_i(QS) r | \hat{O} | F_{i'}(Q'S') r' \rangle_N \end{aligned} \quad (1.39)$$

After taking into account which subspaces  $F_i(QS)$  and  $F_{i'}(Q'S')$  are connected by operator  $\hat{O}$  and performing the sums over  $\alpha$  and  $\beta$ , it turns out that for given  $(QS)$  and  $(Q'S')$  subspaces, only a small number of  $(ii')$  combinations contribute. We finally write

$$\langle QS\omega | \hat{O} | Q'S'\omega' \rangle_{N+1} = \sum_{ii'} C(QS, Q'S', ii') \sum_{rr'} U_{QS}(\omega, ri) U_{Q'S'}(\omega', r'i') \langle F_i(QS) r | \hat{O} | F_{i'}(Q'S') r' \rangle_N. \quad (1.40)$$

The coefficients  $C_{QS, Q'S', ii'}$  are computed using a computer algebra system and they are tabulated in the Appendix. The corresponding routines in “NRG Ljubljana” are `recalc_singlet`, `recalc_doublet` and `recalc_triplet`; they all call a low-level routine `recalc_general` which performs the actual computation. The coefficient tables can be found in files `*-singlet.cpp` (for singlet operators), `*-doublet*.cpp` (for doublet operators) and `*-triplet*.cpp` (for triplet operators).

## Chapter 2

# NRG - User's Manual

### 2.1 Nomenclature

In the single-channel case, the impurity site is denoted by  $d$ , and the conduction band (or, more accurately, the first site of the corresponding Wilson chain) by  $f_0$ . When additional impurities are added, they are named  $a, b, c, e$ . In the two-channel case, the conduction bands are  $f_0$  and  $f_1$ . Note that  $f_0$  is the first site of the Wilson chain of the first band, while  $f_1$  is the first site of the Wilson chain of the second band. In particular,  $f_1$  is *not* the second site of the Wilson chain. If  $\alpha = 1, 2$  is a band index and  $j = 0, 1, 2, \dots$  the site index along the Wilson chain, and we denote the Wilson chain operators by  $g_{\alpha,j}$ , then  $f_0 \equiv g_{1,0}$  and  $f_1 \equiv g_{2,0}$ .

### 2.2 Running the NRG code

First we need to call Mathematica and generate the “data file”, which will contain the eigenvalues of the initial Hamiltonian, irreducible matrix elements  $\langle Q S r \| f^\dagger \| Q' S' r' \rangle$  and irreducible matrix elements for each singlet/doublet/triplet operator that we wish to evaluate. The program must be called from the command line with

```
./nrg -d [-p paramfile]
```

Here `-d` indicates that we are generating the data file. Mathlink is used in this case to run the Mathematica code. The default file name for the parameters file is `param`. The file name of the generated “data file” is by default `data`, but it can be overridden by a setting in the parameters file. Output file `mma1og` containing output from Mathematica is also generated; it should be inspected to see if the problem setup was successful.

The NRG program proper takes in the same paramfile as input, but expects the suitable datafile to be prepared in advance. A suitable call would be

```
./nrg [-p paramfile] [>1og] [2>1og2]
```

It might be a good idea to redirect stdout to a file, because it contains interesting information about the NRG iteration, such as  $(Q, S)$  of the ground state. stderr can be used to follow how the iteration proceeds.

### 2.3 Parameters file

All lines starting with `#` are ignored. Sections start with `[section name]`. There are currently two sections: `[param]`, where parameters from tables 2.1, 2.2 and 2.3 are set, and section

[**extra**] where additional model parameters are set (see tables 2.8, 2.9, 2.10). The syntax is **keyword=value**.

Note that both keywords and values are **case-sensitive**! There is currently little syntax checking, so be careful! All settings, as parsed by the program, are dumped to standard output, where they may (and perhaps should) be checked for correctness.

Parameter	Type	Default	Description
<code>model</code>	string	SIAM	Model (Hamiltonian). See tables 2.8, 2.9 and 2.10. Generally, this sets the number of interacting sites, the topology and the coupling to the leads.
<code>variant</code>	string		Variant of the Hamiltonian. This sets, for example, additional interaction terms. See the tables.
<code>channels</code>	int	1	Number of channels. Currently 1 or 2.
<code>discretization</code>	string	Wilson	The discretization scheme: possible values are <code>Wilson</code> , <code>Yoshida</code> and <code>Campo</code> . The first corresponds to the original Wilson's discretization, the second is the $z$ -shifted discretization due to Yoshida et al., and the last is the discretization based on an over-complete basis due to Campo et al. The recommended discretization scheme is <code>Campo</code> .
<code>z</code>	double	1.0	The value of parameter $z$ in <code>Yoshida</code> and <code>Campo</code> logarithmic discretization schemes.
<code>band</code>	string	<code>flat</code>	The type of the conduction band, i.e. the energy dependence of the density of states. The default <code>flat</code> corresponds to a constant density of states, $\rho = 1/(2D)$ . Other possibilities are <code>cosine</code> and <code>dmft</code> .
<code>ops</code>	string		Which operators should be considered? See table 2.7.
<code>mixed</code>	bool	false	Calculate out-of-diagonal spectral functions, such as $A_{ab}$ . Note: this parameters only takes effect if more than one doublet operators is selected in <code>ops</code> .
<code>Nmax</code>	int	50	Number of NRG iteration steps taken.
<code>Lambda</code>	double	1.0	Logarithmic discretization parameter. $\Lambda = 1.5$ is suitable for calculation of spectral densities, $\Lambda = 2$ for most other (thermodynamic) calculations in the 1-channel case. If <code>discretization=Campo</code> is used, $\Lambda$ can be increased to very high values if the $z$ -trick averaging is used.
<code>betabar</code>	double	0.460	$\bar{\beta}$ , this sets the temperature in the thermodynamic calculations. See Ref. 2.
<code>keep</code>	int	100	Maximum number of eigenstates to be kept at each stage. <code>keep</code> should be increased as much as possible.
<code>keepmin</code>	int	-1	The minimum number of states to be kept at each stage. <code>keepmin</code> < <code>keep</code> .
<code>keepenergy</code>	double	<0	If <code>keepenergy</code> >0, the energy cut-off truncation scheme is used: only the eigenstates with the (rescaled) energy below the value of <code>keepenergy</code> will be retained. This is used in conjunction with <code>keep</code> which sets the maximal number of states kept irrespective of their energy, and <code>keepmin</code> which sets the minimal number of states kept irrespective of their energy. The use of the energy cut-off truncation scheme is recommended, since a high number of states is kept when the degeneracy is high, and a low number when the degeneracy is low; in this fashion, the computational time is divided optimally between the iterations.
<code>safeguard</code>	double	0	Eigenstates in NRG tend to be clustered. Setting <code>safeguard</code> to a finite value enforces retention of additional states, so that the "gap" from the highest retained to the lowest discarded state is at least <code>safeguard</code> . A small value should be used, for example 0.001.

Table 2.1: Parameters for NRG program, section [param].

Parameter	Type	Default	Description
<code>strategy</code>	string	all	Determines which eigenstates are used in the computation of expectation values and spectral functions. If the default setting <code>strategy=all</code> is used, all eigenstates are used. This increases accuracy, but is slow. If <code>strategy=kept</code> is used, only those eigenstates are used that will be kept after truncation. This mode of operation is much faster, since a smaller number of the irreducible matrix elements needs to be recomputed.
<code>Almabda</code>	bool	false	If $\Lambda$ correction is enabled, $\Gamma$ is multiplied by $A(\Lambda) = \frac{1}{2}(1 + \Lambda^{-1})/(1 - \Lambda^{-1}) \log \Lambda$ . This is needed to compare the discretized model with the original continuous Hamiltonian precisely. Note that $A(2) = 1.04$ , so for low $\Lambda$ this correction is not necessary. For <code>discretization=Wilson</code> and <code>discretization=Yoshida</code> , this correction must be used. For <code>discretization=Campo</code> , the correction must <i>not</i> be used.
<code>loggauss_b</code>	double	0.3	Width of logarithmic Gaussians used in broadening of the spectra: $g_n \delta(\omega - \omega_n) \rightarrow g_n \frac{e^{-b^2/4}}{b\omega_n\sqrt{\pi}} \exp\left[-\frac{(\ln \omega - \ln \omega_n)^2}{b^2}\right]$ . Values in the range $0.3 \leq b \leq 0.6$ should be used.
<code>lorentz_b</code>	double	0.6	Prefactor for Lorentzian broadening for frequencies $\omega < \text{limitLL } T$ (for finite temperature dynamic calculations).
<code>limitLL</code>	double	4.0	Sets the limiting energy <code>limitLL</code> $T$ below which Lorentzian broadening is used. By setting this value to 0, we can disable Lorentzian broadening altogether. This is useful for effective “ $T = 0$ ” calculations.
<code>finite</code>	bool	false	Do finite-temperature calculations using the Costi, Hewson, Zlatić approach <sup>115</sup> ?
<code>dmnrg</code>	bool	false	Do the density-matrix numerical renormalization group calculation <sup>120</sup> ? Currently implemented only for 1-channel problems.
<code>goodE</code>	double	2.5	Energy $\omega = \text{goodE } \omega_n$ at which the spectral density is evaluated. Value 2.5 is fine for 1-channel calculations, but it might need to be lowered for 2-channel calculations due to the higher degeneracy which lowers the interval of energies, where spectral information is valid. We should choose as large a <code>goodE</code> as possible, if the range of reliable states is large enough.
<code>mesh</code>	int	10	Extra points used to evaluate the spectral density. Energy points used are $\epsilon_i = \text{goodE } \omega_n \Lambda^{i/\text{mesh}}$ with $i = 0, \dots, \text{mesh} - 1$ .
<code>discardfactor</code>	double	$10^{-7}$	Delta peaks with weight lower than <code>discardfactor</code> $\omega_n$ will be discarded. This can reduce memory usage and execution time.
<code>discardtolerance</code>	double	0.01	If too much cumulative spectral density is discarded, program will abort. This value should be increased for DM-NRG (4-5%), where spectral density may be lost due to round-off errors.

Table 2.2: Continued. Parameters for NRG program, section [param].

Parameter	Type	Default	Description
<code>broaden_max</code>	double	2.5	
<code>broaden_min</code>	double		
<code>broaden_ratio</code>	double	1.05	These three parameters set the mesh of energy points used to obtain the continuous spectral density using the $N/N + 2$ trick. The default values should usually be used.
<code>dumpenergies</code>	bool	false	Dump all energies to a file.
<code>dumpannotated</code>	bool	false	Dump all eigenstates in the form of (quantum numbers) (energy) pairs.
<code>trace</code>	bool	false	Trace the NRG iteration: output files are named <code>NNN.energies</code> .
<code>loglabel</code>	string	<code>delta</code>	Which variable should be used to label results in output files? This should be used in parameter sweeps to obtain a suitable first column.
<code>rawpeaks</code>	bool	false	Save all $(g_n, \omega_n)$ pairs calculated in the spectral density calculations. This is useful for testing various peak broadening procedures and for troubleshooting.
<code>factorextra</code>	double	1.0	
<code>Nextra</code>	int	-1	The value of <code>keep</code> can be increased by a factor of <code>factorextra &gt; 1</code> after <code>Nextra</code> steps. This way it is possible to achieve better spectral resolution at very low frequencies. This may help to obtain better $A(\omega)$ , which is used in conductance calculation using Meir-Wingreen formula.
<code>data</code>	string	<code>data</code>	File containing the information about the initial Hamiltonian (eigenstates, irreducible matrix elements for the Wilson's chain and for operators defined on the impurity).
<code>verbose</code>	bool	false	Increases verbosity level. Can be useful for debugging, but also for getting more information about the physical system.
<code>log</code>	string		What information to dump to the standard output. See Table 2.5.
<code>mmadebug</code>	int	0	Set the level of diagnostic messages in the Mathematica part of the program. The output file is called <code>mma1og</code> . Use of value $\geq 1$ is recommended.
<code>diag</code>	string	<code>dsyev</code>	Choose the diagonalization routine. Either <code>dsyev</code> or <code>dsyevr</code> LAPACK routines can be used. The latter makes possible to calculate only a finite number of eigenstates for each Hamiltonian matrix.
<code>diagratio</code>	double	1.0	The ratio of the eigenstates computed using the <code>dsyevr</code> routine. This value should, in principle, be set somewhat above 0.25 for one-channel problems, and above 0.0625 for two-channel problems. Depending on the problem, larger values might actually be necessary in order to avoid systematic errors.
<code>dsyevrlimit</code>	int	100	The minimal size of the matrix for diagonalization using the <code>dsyevr</code> routine.
<code>options</code>	string		Additional options that are passed to the Mathematica part of the program. They are listed in Table 2.6.
<code>perturb</code>	string		An arbitrary string that is added to the Hamiltonian expression. This may be used for trying out the effect of various perturbations to the model Hamiltonian.
<code>calc0</code>	bool	false	Perform calculation of physical quantities at the initial (0-th) NRG step, i.e. before the first NRG iteration.

Table 2.3: Continued. Parameters for NRG program, section [param].

Parameter	Term in Hamiltonian	Description
$\delta$ ( <b>delta</b> )	$\delta(\hat{n} - 1)$	Deviation from particle-hole symmetric point (if the selected model has such symmetry at all!). Related to gate-voltage by $\epsilon_d = \delta - U/2$ .
$U$ ( <b>U</b> )	$U\hat{n}_\uparrow\hat{n}_\downarrow \rightarrow U/2(\hat{n} - 1)^2$	On-site electron-electron repulsion.
$\Gamma$ ( <b>Gamma</b> )		Coupling to the leads.

Table 2.4: Mandatory parameters in all models.

Token	Description
d	Diagonalization process (low-level information)
i	Iteration process (subspaces, timing, ...)
e	Dump eigenvalues in function <code>diagonalize()</code> . Up to <code>lognumber</code> values are dumped.
m	Dump Hamiltonian matrix of each subspace
s	Dump ancestor subspaces during the construction of the Hamiltonian matrix
x	Dump values of <code>xi()</code>
X	Dump values of <code>XbXf()</code>
f	Follow the recalculation in function <code>recalc_f</code>
r	Follow the recalculation in function <code>recalc_general</code>
g	Details about the DM-NRG run
a	Details about the deta file
c	Details about the spectral density calculation
!	Full details about the spectral density calculation

Table 2.5: The tokens to be used to specify the level of logging. The tokens must be given successively as the value of parameter `log`. For example, use `log=di` to log the details of the diagonalization process and the NRG iterations.

Option	Description
READXI	Read the values of coefficients <code>xi</code> from files.
READBASIS	Read the basis states from files.
READHAM	Read the Hamiltonians from files.

Table 2.6: The options for `options` setting in the parameter file. These values are passed to the Mathematica part of the program for low-level tweaking.

## 2.4 Operators

Note that a “singlet operator” must be symmetric under all symmetry groups taken into account in the calculation and be, furthermore, a singlet tensor operator with respect to all the symmetry groups. For example,  $\hat{n}^2$  is not isospin symmetric, while  $(\hat{n} - 1)^2$  is.

Name	Operator	Description
n_i	$n_i = n_{\uparrow i} + n_{\downarrow i}$	Occupation number. $i \in f, d, a, b$
n_i^2	$n_i^2 = (n_{\uparrow i} + n_{\downarrow i})^2 = n_{\uparrow i} + n_{\downarrow i} + 2n_{\uparrow i}n_{\downarrow i}$	Occupation number squared
q_i	$q_i = n_{\uparrow i} + n_{\downarrow i} - 1$	Occupation number with respect to half-filling.
q_i^2	$q_i^2$	Charge fluctuation in the particle-hole symmetric case.
n_in_j	$n_i n_j$	Inter-site product of occupation number operators. These are required to calculate the total charge fluctuation from formula $\langle N^2 \rangle - \langle N \rangle^2$ , where $N = \sum_i n_i$ .
ntot	$\sum_i n_i$	The total occupancy of impurities. Index $i$ in the sum ranges over impurity sites only (i.e. $d, a, b$ , etc.).
ntot^2	$(\sum_i n_i)^2$	The square of the total impurity occupancy.
s^2	$(\sum_i \mathbf{S}_i)^2$	The square of the total impurity spin. Index $i$ in the sum ranges over impurity sites only.
q_i q_j	$q_i q_j$	Intersite product of occupation number operators (wrt half-filling).
A_i	$\text{Im } G_i^R(\omega)$	Spectral density. A_i actually enables calculation of doublet operator $i^\dagger$ . This is then used in various evaluations of spectral density.
sigma_i	$\Sigma_i(t) = \langle S_z(t) S_z(0) \rangle$	Calculate dynamic spin susceptibility. This enables calculation of triplet operator $\sigma_i$ , which is then used in evaluations of spectral density.
P0	$(n_{\uparrow, d} - 1)(n_{\downarrow, d} - 1)$	Projector to zero occupancy subspace. [QSZ]
Pu	$n_{\uparrow, d}(n_{\downarrow, d} - 1)$	Projector to spin-up occupancy subspace. [QSZ]
Pd	$n_{\downarrow, d}(n_{\uparrow, d} - 1)$	Projector to spin-down occupancy subspace. [QSZ]
P2	$n_{\uparrow, d} n_{\downarrow, d}$	Projector to double occupancy subspace. [QSZ]
SZd	$S_d^z$	The spin component along the $z$ -axis. [QSZ]
SZ2d	$(S_d^z)^2$	The spin component along the $z$ -axis squared. [QSZ]
SdSd	$\mathbf{S}_d^2$	Local spin squared.
SdSf	$\mathbf{S}_d \cdot \mathbf{S}_f$	Spin-spin correlation function.

Table 2.7: Operators known to `initial.m`

Model	Variant	Description	Additional parameters
CLEAN	-	No impurities.	
SIAM	-	Single-impurity Anderson model. The impurity site (dot) is indexed $d$ . $H_{\text{SIAM}} = \delta(n_d - 1) + U/2(n_d - 1)^2$ $\left[ +\sqrt{\Gamma} \left( f_{0\sigma}^\dagger d_\sigma + \text{H.c.} \right) \right]$	
	MAGFIELD	Anderson impurity in magnetic field. $H_{\text{SIAM}} + BS_d^z$	B
SIDE	-	DQD, side-coupled configuration. The side-coupled dot is indexed $a$ . $H_{\text{SIDE}} = H_{\text{SIAM}} + \delta(n_a - 1) + U/2(n_a - 1)^2 + t(a_\sigma^\dagger d_\sigma + \text{H.c.})$	$\mathbf{t}$
	MAGFIELD	Side-coupled DQD in magnetic field. $H_{\text{SIDE}} + B(S_a^z + S_d^z)$	$\mathbf{t}, \mathbf{B}$
	DNI	Central dot $d$ is non-interacting, but it feels the gate voltage $\delta(n_d - 1) + \delta(n_a - 1) + U/2(n_a - 1)^2 + t(a_\sigma^\dagger d_\sigma + \text{H.c.})$	$\mathbf{t}$
	Uad	Model SIDE + charge-coupling between sites $a$ and $d$ $H_{\text{SIDE}} + U_{ad}(n_a - 1)(n_d - 1)$	$\mathbf{t}, \text{Uad}$
	Jad	Model SIDE + spin-coupling between sites $a$ and $d$ $H_{\text{SIDE}} + J_{ad}\mathbf{S}_a \cdot \mathbf{S}_d$	$\mathbf{t}, \text{Jad}$
	Tad	Model SIDE + electron pairing interaction (two-electron hopping) between sites $a$ and $d$ $H_{\text{SIDE}} + T_{ad}(a_\uparrow^\dagger a_\downarrow^\dagger d_\uparrow d_\downarrow + \text{H.c.})$	Tad

Table 2.8: Models and variants provided as examples in `initial.m` and `models.m`. The list is not complete: see the cited files for additional model definitions. **Single-channel, one/two-impurity problems.**

Model	Variant	Description	Additional parameters
RING	-	Ring consisting of two dots, $d$ and $a$ , coupled symmetrically to two leads. $(\delta + \text{deltaeps})(n_d - 1) + U/2(n_a - 1)^2 + (\delta - \text{deltaeps})(n_a - 1) + U/2(n_a - 1)^2$ $\left[ +\sqrt{\Gamma} \left( f_{0\sigma}^\dagger d_\sigma + f_{0\sigma}^\dagger a_\sigma + \text{H.c.} \right) \right]$	deltaeps
	INVERSESIGN	One $U$ is positive, the other is negative $(\delta + \text{deltaeps})(n_d - 1) + U/2(n_a - 1)^2 + (\delta - \text{deltaeps})(n_a - 1) - U/2(n_a - 1)^2$	deltaeps
	tad	Electron hopping between sites $a$ and $d$ . $(\delta + \text{deltaeps})(n_d - 1) + U/2(n_a - 1)^2 + (\delta - \text{deltaeps})(n_a - 1) + U/2(n_a - 1)^2 + t_{ad}(d_\sigma^\dagger a_\sigma + \text{H.c.})$	deltaeps, tad
	Uad	Charge-coupling between sites $a$ and $d$ $(\delta + \text{deltaeps})(n_d - 1) + U/2(n_a - 1)^2 + (\delta - \text{deltaeps})(n_a - 1) + U/2(n_a - 1)^2 + U_{ad}(n_d - 1)(n_a - 1)$	deltaeps, Uad

Table 2.9: Continued. **Single-channel ring model and tripple quantum dot.**

Model	Variant	Description	Additional parameters
ONE	SIAM	<i>Two-channel, one-site problems</i> Single impurity Anderson model $H_{\text{SIAM}} \left[ + \sum_{i=L,R} \sqrt{\Gamma/2} \left( f_{0\sigma i}^\dagger d_\sigma + \text{H.c.} \right) \right]$	
THREE	NEWTQD	<i>Two-channel, three-sites problems</i> Symmetric linear chain $\sum_{i=a,b,d} \delta(n_i - 1) + U/2(n_i - 1)^2 + t'' (a_\sigma^\dagger d_\sigma + d_\sigma^\dagger b_\sigma + \text{H.c.})$ $\left[ + \sqrt{\Gamma} \left( f_{0\sigma L}^\dagger a_\sigma + f_{0\sigma R}^\dagger b_\sigma + \text{H.c.} \right) \right]$	tpp

Table 2.10: Continued. **Two-channel models.**

Filename	Description
<code>chi</code>	Impurity contribution to magnetic susceptibility, thermodynamic expectation values $\langle S_z^2 \rangle$ , $\langle S_z \rangle^2$ , and $\langle Q \rangle$ , entropy, free energy, heat capacity, etc.
<code>annotated.dat</code>	NRG eigenvalue spectra as { value, quantum numbers } pairs.
<code>cond</code>	Conductance at the lowest temperature: <ul style="list-style-type: none"> <li>• <code>A(w)</code>, <code>FR</code> - Friedel sum rule from spectrum (only makes sense at <math>T=0</math>)</li> <li>• <code>pts</code>, <code>MW</code> - Conductance from spectral density and Meir-Wingreen formula</li> </ul>
<code>custom</code>	Temperature dependent thermodynamic expectation values of selected operators
<code>cust</code>	As above, but for the lowest temperature only. Instead of the temperature, however, the first column is the value of the parameter selected by <code>label</code> in the parameters file, which is <code>delta</code> by default. This file is used to facilitate gathering of the results of parameter sweeps.
<code>data</code>	Input file for NRG iteration (generated by Mathematica)
<code>dmnrg</code>	Statistics about density matrices.
<code>report.*</code>	Debugging information, such as initial eigenvalues.
<code>spec_TYPE_[dens pts]_OP.dat</code>	Spectral density corresponding to operator <code>OP</code> , which can be <code>A_i-A_i</code> for local density of states, <code>A_i-A_j</code> for the imaginary part of the symmetrized out-of-diagonal components of the retarded Green's function, or <code>sigma_i</code> for dynamic spin susceptibility. <ul style="list-style-type: none"> <li>• <code>TYPE=T0</code> - "zero temperature" spectral density</li> <li>• <code>TYPE=FT</code> - finite temperature spectral density</li> <li>• <code>TYPE=DMNRG</code> - spectral density calculated using density-matrix NRG</li> <li>• <code>TYPE=spin</code> - dynamic spin susceptibility</li> <li>• <code>dens</code> = <math>N/N+2</math> trick for obtaining smooth spectra</li> <li>• <code>pts</code> = raw, rougher spectrum</li> </ul>

Table 2.11: Output files and their contents

## 2.5 Adding new models

Additional models are to be defined in `models.m` or, preferably, in `custommodels.m`. At the very least, the model definition should define the number of impurity sites `NRDOTS`, and the Hamiltonian `H`. Some default Hamiltonian definitions are assigned to `H1` and `Hc` in `initial.m`, so that `H1` is the single-impurity Anderson model (impurity part) and `Hc` is the coupling term (electron hopping from the impurity to the band). Different models can then be defined by adding to `H1` and `Hc`, or by overriding these definitions altogether.

If `ISO` or `ISOLR` symmetry type is used, the lattice indexes must be set up correctly using `nnop`, so that even-indexed sites correspond to one sublattice and odd-indexed sites to the other sublattice of the bipartite lattice (it should be recalled that the isospin symmetry can only exist for lattices that are bipartite with respect to the electron hopping).

If `ISOLR` or `QSLR` symmetry type is used, the left-right correspondence must be defined with list `lrchain`. The principle here is that operators in this list correspond to operators in the reversed list. For example, if `lrchain={ f[0], a[], b[], f[1] }`, then `f[0]` is paired with `f[1]`, and `a[]` is paired with `b[]`.

If `BASISRULE` is defined, the operator given is applied to each basis state in turn. The obtained basis is then orthonormalized. Using this approach, certain unneeded subspaces can be projected out. For example, the Hilbert space of the Kondo model can be defined using a `d[]` orbital with zero and double occupancy subspaces projected out, so that only the two single-occupancy states with spin up and down remain.

If a new parameter is introduced, it should be added to the list `params` that is defined at the beginning of `models.m`. The general rule is that for a new parameter `x`, a line such as `x -> faktor extrax` should be added. Here `faktor` is needed, since the Hamiltonian is rescaled before the NRG iteration is started. The prefix `extra` is needed, because it is automatically prepended to each parameter defined in section `[extra]` of the parameters file to avoid "name-space collision".

## 2.6 Adding new operators

Additional operators are to be defined in file `operators.m` or, preferably, in `customoperators.m`. The defining operator expressions can be expressed using the operators of the second quantization using the helper functions of the `sneg` Mathematica package such as `number`, `spinspin`, `hop`, `chargecharge`, etc. Consult the documentation and the source of the package `sneg` for details.

# Appendix A

## Recursion relation coefficients

$i$	$i'$	$C(QS, Q'S', ii')$	$i$	$i'$	$C(QS, Q'S', ii')$
1	1	1	1	1	1
2	2	$-\frac{2\sqrt{S(S+1)}}{2S+1}$	2	2	-1
3	2	$\frac{1}{2S+1}$	2	3	$-\frac{1}{2S+1}$
3	3	-1	3	3	$-\frac{2\sqrt{S(S+1)}}{2S+1}$
4	4	1	4	4	1

(a)  $Q' = Q - 1, S' = S + \frac{1}{2}$

(b)  $Q' = Q - 1, S' = S - \frac{1}{2}$

Table A.1: Coefficients in the recursion relations for doublet operator in one-channel problems

$i$	$i'$	$C(QS, Q'S', ii')$	$i$	$i'$	$C(QS, Q'S', ii')$
1	1	1	1	1	1
2	2	$\frac{2\sqrt{S(1+S)}}{1+2S}$	2	2	-1
3	2	$\frac{1}{1+2S}$	2	3	$-\frac{1}{1+2S}$
3	3	-1	3	3	$-\frac{2\sqrt{S(1+S)}}{1+2S}$
4	4	$-\frac{2\sqrt{S(1+S)}}{1+2S}$	4	4	-1
5	4	$\frac{1}{1+2S}$	4	5	$-\frac{1}{1+2S}$
5	5	-1	5	5	$-\frac{2\sqrt{S(1+S)}}{1+2S}$
6	6	1	6	6	1
7	7	1	7	7	1
8	8	1	8	8	1
9	9	$\sqrt{1 - \frac{1}{S} + \frac{1}{\frac{1}{2}+S}}$	9	9	1
10	9	$-\frac{1}{\sqrt{S(1+2S)}}$	9	10	$\frac{1}{\sqrt{S(1+2S)}}$
10	10	$\frac{3+2S}{\sqrt{(1+S)(1+2S)(3+2S)}}$	10	10	$\frac{-1+S+2S^2}{\sqrt{S(1+S)(-1+2S)(1+2S)}}$
11	10	$-\frac{1}{\sqrt{(1+S)(1+2S)}}$	10	11	$\frac{1}{\sqrt{(1+S)(1+2S)}}$
11	11	1	11	11	$\sqrt{1 + \frac{1}{1+S} - \frac{2}{1+2S}}$
12	12	$-\frac{2\sqrt{S(1+S)}}{1+2S}$	12	12	-1
13	12	$\frac{1}{1+2S}$	12	13	$-\frac{1}{1+2S}$
13	13	-1	13	13	$-\frac{2\sqrt{S(1+S)}}{1+2S}$
14	14	$-\frac{2\sqrt{S(1+S)}}{1+2S}$	14	14	-1
15	14	$\frac{1}{1+2S}$	14	15	$-\frac{1}{1+2S}$
15	15	-1	15	15	$-\frac{2\sqrt{S(1+S)}}{1+2S}$
16	16	1	16	16	1

(a)  $Q' = Q - 1, S' = S + \frac{1}{2}$ (b)  $Q' = Q - 1, S' = S - \frac{1}{2}$ 

Table A.2: Coefficients in the recursion relations for doublet operator in two-channel problems

$i$	$i'$	$C(QS, Q'S', ii')$	$i$	$i'$	$C(QS, Q'S', ii')$	$i$	$i'$	$C(QS, Q'S', ii')$
1	1	1	1	1	1	1	1	1
2	2	$\frac{4S^2+4S-1-1/S}{2S+1}$	2	2	$\frac{\sqrt{S(S+1)(2S+1)(2S+3)}}{1+3S+2S^2}$	2	2	1
2	3	$\frac{1}{\sqrt{(S+1)(2S+1)}}$	3	2	$-\frac{1}{\sqrt{(S+1)(2S+1)}}$	2	3	$\frac{1}{\sqrt{S(2S+1)}}$
3	2	$-\frac{1}{\sqrt{S(2S+1)}}$	3	3	1	3	3	$\sqrt{1 - \frac{1}{S} + \frac{2}{2S+1}}$
3	3	$\frac{S\sqrt{2S+3}}{\sqrt{S(S+1)(2S+1)}}$	4	4	1	4	4	1
4	4	1						

(a)  $Q' = Q, S' = S$ (b)  $Q' = Q, S' = S + 1$ (c)  $Q' = Q, S' = S - 1$ 

Table A.3: Coefficients in the recursion relation for triplet operator in one-channel problems

$i$	$i'$	$C(QS, Q'S', ii')$	$i$	$i'$	$C(QS, Q'S', ii')$	$i$	$i'$	$C(QS, Q'S', ii')$
1	1	1	1	1	1	1	1	1
2	2	$\frac{\sqrt{-1-\frac{1}{S}+4S+4S^2}}{1+2S}$	2	2	$\frac{S(3+2S)}{\sqrt{S(1+S)(1+2S)(3+2S)}}$	2	2	1
2	3	$\frac{1}{\sqrt{(1+S)(1+2S)}}$	3	2	$-\frac{1}{\sqrt{(1+S)(1+2S)}}$	2	3	$\frac{1}{\sqrt{S(1+2S)}}$
3	2	$-\frac{1}{\sqrt{S(1+2S)}}$	3	3	1	3	3	$\sqrt{1-\frac{1}{S}+\frac{1}{\frac{1}{2}+S}}$
3	3	$\frac{S}{\sqrt{\frac{S(1+S)(1+2S)}{3+2S}}}$	4	4	$\frac{S(3+2S)}{\sqrt{S(1+S)(1+2S)(3+2S)}}$	4	4	1
4	4	$\frac{\sqrt{-1-\frac{1}{S}+4S+4S^2}}{1+2S}$	5	4	$-\frac{1}{\sqrt{(1+S)(1+2S)}}$	4	5	$\frac{1}{\sqrt{S(1+2S)}}$
4	5	$\frac{1}{\sqrt{(1+S)(1+2S)}}$	5	5	1	5	5	$\sqrt{1-\frac{1}{S}+\frac{1}{\frac{1}{2}+S}}$
5	4	$-\frac{1}{\sqrt{S(1+2S)}}$	6	6	1	6	6	1
5	5	$\frac{S}{\sqrt{\frac{S(1+S)(1+2S)}{3+2S}}}$	7	7	1	7	7	1
6	6	1	8	8	1	8	8	1
7	7	1	9	9	$\frac{\sqrt{-1+S^2}}{S}$	9	9	1
8	8	1	9	10	$\frac{\sqrt{1-\frac{2}{1+2S}}}{S}$	9	10	$\frac{1}{S}$
9	9	$\frac{\sqrt{-1+S^2}}{S}$	10	9	$-\frac{1}{S}$	9	11	$\frac{1}{S+2S^2}$
9	10	$\frac{\sqrt{1-\frac{2}{1+2S}}}{S}$	10	10	$\frac{-1+S+S^2}{S(1+S)}$	10	10	$\frac{\sqrt{-1+S^2}}{S}$
10	9	$-\frac{1}{S}$	10	11	$\frac{1}{1+S}$	10	11	$\frac{\sqrt{1-\frac{2}{1+2S}}}{S}$
10	10	$\frac{-1+S+S^2}{S(1+S)}$	11	9	$\frac{1}{1+3S+2S^2}$	11	11	$\frac{\sqrt{-3+4S(1+S)}}{1+2S}$
10	11	$\frac{1}{1+S}$	11	10	$-\frac{1}{1+S}$	11	11	1
11	10	$-\frac{3+2S}{(1+S)\sqrt{3+4S(2+S)}}$	11	11	1	12	12	1
11	11	$\frac{\sqrt{S(2+S)}}{1+S}$	12	12	$\frac{S(3+2S)}{\sqrt{S(1+S)(1+2S)(3+2S)}}$	12	13	$\frac{1}{\sqrt{S(1+2S)}}$
12	12	$\frac{\sqrt{-1-\frac{1}{S}+4S+4S^2}}{1+2S}$	13	12	$-\frac{1}{\sqrt{(1+S)(1+2S)}}$	13	13	$\sqrt{1-\frac{1}{S}+\frac{1}{\frac{1}{2}+S}}$
12	13	$\frac{1}{\sqrt{(1+S)(1+2S)}}$	13	13	1	14	14	1
13	12	$-\frac{1}{\sqrt{S(1+2S)}}$	14	14	$\frac{S(3+2S)}{\sqrt{S(1+S)(1+2S)(3+2S)}}$	14	15	$\frac{1}{\sqrt{S(1+2S)}}$
13	13	$\frac{S}{\sqrt{\frac{S(1+S)(1+2S)}{3+2S}}}$	15	14	$-\frac{1}{\sqrt{(1+S)(1+2S)}}$	15	15	$\sqrt{1-\frac{1}{S}+\frac{1}{\frac{1}{2}+S}}$
14	14	$\frac{\sqrt{-1-\frac{1}{S}+4S+4S^2}}{1+2S}$	15	15	1	16	16	1
14	15	$\frac{1}{\sqrt{(1+S)(1+2S)}}$	16	16	1			
15	14	$-\frac{1}{\sqrt{S(1+2S)}}$						
15	15	$\frac{S}{\sqrt{\frac{S(1+S)(1+2S)}{3+2S}}}$						
16	16	1						

(a)  $Q' = Q, S' = S$ (b)  $Q' = Q, S' = S + 1$ (c)  $Q' = Q, S' = S - 1$ 

Table A.4: Coefficients in the recursion relation for triplet operator in two-channel problems

# Bibliography

- [1] K. G. Wilson. The renormalization group: Critical phenomena and the Kondo problem. *Rev. Mod. Phys.*, **47** 773, 1975.
- [2] H. R. Krishna-murthy, J. W. Wilkins, and K. G. Wilson. Renormalization-group approach to the Anderson model of dilute magnetic alloys. I. Static properties for the symmetric case. *Phys. Rev. B*, **21** 1003, 1980.
- [3] H. R. Krishna-murthy, J. W. Wilkins, and K. G. Wilson. Renormalization-group approach to the Anderson model of dilute magnetic alloys. II. Static properties for the asymmetric case. *Phys. Rev. B*, **21** 1044, 1980.
- [4] Ralf Bulla, Theo Costi, and Thomas Pruschke. The numerical renormalization group method for quantum impurity systems. *cond-mat/0701106*, 2007.
- [5] P. W. Anderson and G. Yuval. Exact results in the Kondo problem: Equivalence to a classical one-dimensional Coulomb gas. *Phys. Rev. Lett.*, stran 89, 1969.
- [6] G. Yuval and P. W. Anderson. Exact results for the Kondo Problem: One-Body Theory and Extension to Finite Temperature. *Phys. Rev. B*, **1** 1522, 1970.
- [7] P. W. Anderson, G. Yuval, and D. R. Hamann. Exact results in the Kondo problem II: Scaling Theory, Qualitatively correct solution and some new results on one-dimensional classical statistical models. *Phys. Rev. B*, **1** 4464, 1970.
- [8] P. W. Anderson. Basic notions of condensed matter physics. The Benjamin-Cummings Publishing Company, 1984.
- [9] D. M. Cragg and P. Lloyd. Potential scattering and the Kondo problem. *J. Phys. C: Solid State Phys.*, **11** L597, 1978.
- [10] D. M. Cragg and P. Lloyd. Universality and the renormalisability of rotationally invariant Kondo Hamiltonians. *J. Phys. C: Solid State Phys.*, **12** 3301, 1979.
- [11] D. M. Cragg and P. Lloyd. Kondo Hamiltonians with a non-zero ground-state spins. *J. Phys. C: Solid State Phys.*, **12** L215, 1979.
- [12] W. Koller, A. C. Hewson, and D. Meyer. Singular dynamics of underscreened magnetic impurity models. *Phys. Rev. B*, **72** 045117, 2005.
- [13] P. Mehta, N. Andrei, P. Coleman, L. Borda, and G. Zaránd. Regular and singular Fermi-liquid fixed points in quantum impurity models. *Phys. Rev. B*, **72** 014430, 2005.
- [14] D. M. Cragg, P. Lloyd, and P. Nozières. On the ground states of some s-d exchange Kondo Hamiltonians. *J. Phys. C: Solid St. Phys.*, **13** 803, 1980.
- [15] H. B. Pang and D. L. Cox. Stability of the fixed point of the two-channel Kondo Hamiltonian. *Phys. Rev. Lett.*, **44** 9454, 1991.
- [16] I. Affleck, A. W. W. Ludwig, H.-B. Pang, and D. L. Cox. Relevance of anisotropy in the multichannel Kondo effect: Comparison of conformal field theory and numerical renormalization-group results. *Phys. Rev. B*, **45** 7918, 1992.
- [17] H. Kusunose, K. Miyake, Y. Shimizu, and O. Sakai. Numerical renormalization-group study of particle-hole symmetry breaking in two-channel Kondo problem: Effect of repulsion among conduction electrons and potential scattering. *Phys. Rev. Lett.*, **76** 271, 1996.
- [18] D. L. Cox and A. Zawadowski. Exotic Kondo effects in metals: magnetic ions in a crystalline electric field and tunneling centres. *Adv. Phys.*, **47** 599, 1998.
- [19] H. R. Krishna-murthy, J. W. Wilkins, and K. G. Wilson. Temperature-Dependent Susceptibility of the Symmetric Anderson Model: Connection to the Kondo Model. *Phys. Rev. Lett.*, **35** 1101, 1975.
- [20] O. Sakai, Y. Shimizu, and T. Kasuya. Single-particle and magnetic excitation spectra of degenerate Anderson model with finite f-f Coulomb interaction. *J. Phys. Soc. Japan*, **58** 3666, 1989.

- [21] Michele Fabrizio, Andrew F. Ho, Lorenzo De Leo, and Giuseppe E. Santoro. Nontrivial fixed point in a twofold orbitally degenerate Anderson impurity model. *Phys. Rev. Lett.*, **91** 246402, 2003.
- [22] Lorenzo De Leo and Michele Fabrizio. Spectral properties of a two-orbital Anderson impurity model across a non-Fermi-liquid fixed point. *Phys. Rev. B*, **69**(24) 245114, 2004.
- [23] A. K. Zhuravlev, V. Yu. Irkhin, M. I. Katsnelson, and A. I. Lichtenstein. Kondo Resonance for Orbitally Degenerate Systems. *Phys. Rev. Lett.*, **93**(23) 236403, 2004.
- [24] R. Allub, H. Ceva, and B. R. Alascio. Magnetic susceptibility of a model for valence fluctuations between two magnetic configurations: Renormalization-group approach. *Phys. Rev. B*, **29** 3098, 1984.
- [25] C. Jayaprakash, H. R. Krishna-murthy, and J. W. Wilkins. Two-impurity Kondo problem. *Phys. Rev. Lett.*, **47** 737, 1981.
- [26] B. A. Jones and C. M. Varma. Study of Two Magnetic Impurities in a Fermi Gas. *Phys. Rev. Lett.*, **58** 843, 1987.
- [27] B. A. Jones, C. M. Varma, and J. W. Wilkins. Low-temperature properties of the two-impurity Kondo Hamiltonian. *Phys. Rev. Lett.*, **61** 125, 1988.
- [28] J. B. Silva, W. L. C. Lima, W. C. Oliveira, J. L. N. Mello, L. N. Oliveira, and J. W. Wilkins. Particle-Hole asymmetry in the Two-Impurity Kondo model. *Phys. Rev. Lett.*, **76** 275, 1996.
- [29] O. Sakai and Y. Shimizu. Excitation spectra of two impurity Anderson model. I. Critical Transition in the Two Magnetic Impurity Problem and the Roles of the Parity Splitting. *J. Phys. Soc. Japan*, **61** 2333, 1992.
- [30] C. A. Paula, M. F. Silva, and L. N. Oliveira. Low-energy spectral density for the Alexander-Anderson model. *Phys. Rev. B*, **59** 85, 1999.
- [31] R. Žitko, J. Bonča, A. Ramšak, and T. Rejec. Kondo effect in triple quantum dots. *Phys. Rev. B*, **73** 153307, 2006.
- [32] Rok Žitko and Janez Bonča. Fermi-liquid versus non-Fermi-liquid behavior in triple quantum dots. *cond-mat/0606287*, 2006.
- [33] D. Meyer, A. C. Hewson, and R. Bulla. Gap formation and soft phonon mode in the Holstein model. *Phys. Rev. Lett.*, **89** 196401, 2002.
- [34] A. C. Hewson and D. Meyer. Numerical renormalization group study of the Anderson-Holstein model. *J. Phys. - Condens. Mat.*, **14** 427, 2002.
- [35] Gun Sang Jeon, Tae-Ho Park, and Han-Yong Choi. Numerical renormalization-group study of the symmetric Anderson-Holstein model: Phonon and electron spectral functions. *Phys. Rev. B*, **68** 045106, 2003.
- [36] P. S. Cornaglia, H. Ness, and D. R. Grempel. Many-Body Effects on the Transport Properties of Single-Molecule Devices. *Phys. Rev. Lett.*, **93** 147201, 2004.
- [37] P. S. Cornaglia and D. R. Grempel. Magnetoconductance through a vibrating molecule in the Kondo regime. *Phys. Rev. B*, **71** 245326, 2005.
- [38] R. Bulla, Hyun-Jung Lee, Ning-Hua Tong, and Matthias Vojta. Numerical renormalization group for quantum impurities in a bosonic bath. *Phys. Rev. B*, **71** 045122, 2005.
- [39] K. Chen and C. Jayaprakash. X-ray-edge singularities with nonconstant density of states: A renormalization-group approach. *Phys. Rev. B*, **52** 14436, 1995.
- [40] Kevin Ingersent. Behavior of magnetic impurities in gapless Fermi systems. *Phys. Rev. B*, **54** 11936, 1996.
- [41] R. Bulla, Th. Pruschke, and A. C. Hewson. Anderson impurity in pseudo-gap Fermi systems. *J. Phys.: Condens. Matter.*, **9** 10463, 1997.
- [42] Kan Chen and C. Jayaprakash. Kondo effect in Fermi systems with a gap: A renormalization-group study. *Phys. Rev. B*, **57** 5225, 1998.
- [43] Carlos Gonzalez-Buxton and Kevin Ingersent. Renormalization-group study of Anderson and Kondo impurities in gapless Fermi systems. *Phys. Rev. B*, **57** 14254, 1998.
- [44] Ralf Bulla, Matthew T Glossop, David E Logan, and Thomas Pruschke. The soft-gap Anderson model: comparison of renormalization group and local moment approaches. *J. Phys.: Condens. Matter*, **12** 4899, 2000.
- [45] Tae-Suk Kim, L. N. Oliveira, and D. L. Cox. Non-Fermi-liquid fixed point. *Phys. Rev. B*, **55** 12460, 1997.
- [46] R. Bulla, A. C. Hewson, and G.-M. Zhang. Low-energy fixed points of the  $\sigma$ - $\tau$  and the O(3) symmetric Anderson models. *Phys. Rev. B*, **56** 11721, 1997.

- [47] M. Koga, G. Zaránd, and D. L. Cox. Crystal Field Triplets: A new route to non-fermi-liquid physics. *Phys. Rev. Lett.*, **83** 2421, 1999.
- [48] M. Koga. Hidden non-Fermi-liquid behavior due to a crystal-field quartet. *Phys. Rev. B*, **61** 395, 2000.
- [49] Matthias Vojta and Ralf Bulla. Kondo effect of impurity moments in d-wave superconductors: Quantum phase transitions and spectral properties. *Phys. Rev. B*, **65** 014511, 2002.
- [50] Mikito Koga and Masashige Matsumoto. Nonvanishing Local Moment in Triplet Superconductors. *J. Phys. Soc. Japan*, **71** 943, 2002.
- [51] M. Vojta, R. Bulla, and W. Hofstetter. Quantum phase transitions in models of coupled magnetic impurities. *Phys. Rev. B*, **65** 140405(R), 2002.
- [52] Matthias Vojta. Quantum phase transitions. *Rep. Prog. Phys.*, **66** 2069, 2003.
- [53] W. Izumida, O. Sakai, and Y. Shimizu. Kondo effect in single quantum dot systems – Study with Numerical Renormalization Group Method. *J. Phys. Soc. Japan*, **67** 2444, 1998.
- [54] W. Hofstetter and J. König and H. Schoeller. Kondo Correlations and the Fano Effect in Closed Aharonov-Bohm Interferometers. *Phys. Rev. Lett.*, **87** 156803, 2001.
- [55] D. Boese, W. Hofstetter, and H. Schoeller. Interference and interaction effects in multilevel quantum dots. *Phys. Rev. B*, **64** 125309, 2001.
- [56] W. Izumida and O. Sakai. Kondo Effect in Quantum Dot Systems – Numerical Renormalization Group Study. *J. Phys. Soc. Japan*, **74** 103, 2005.
- [57] Wataru Izumida, Osamu Sakai, and Yukihiko Shimizu. Many body effects on electron tunneling through quantum dots in an Aharonov-Bohm circuit. *J. Phys. Soc. Japan*, **66** 717, 1997.
- [58] W. Izumida and O. Sakai. Two-impurity Kondo effect in double-quantum-dot systems: Effect of interdot kinetic exchange coupling. *Phys. Rev. B*, **62** 10260, 2000.
- [59] D. Boese, W. Hofstetter, and H. Schoeller. Interference in interacting quantum dots with spin. *Phys. Rev. B*, **66** 125315, 2002.
- [60] P. S. Cornaglia and D. R. Grempel. Strongly correlated regimes in a double quantum dot device. *Phys. Rev. B*, **71** 075305, 2005.
- [61] M. R. Galpin, D. E. Logan, and H. R. Krishnamurthy. Quantum phase transition in capacitively coupled double quantum dot. *Phys. Rev. Lett.*, **94** 186406, 2005.
- [62] M. Sindel, A. Silva, Y. Oreg, and J. von Delft. Charge oscillations in quantum dots: Renormalization group and Hartree method calculations. *Phys. Rev. B*, **72** 125316, 2005.
- [63] Martin R. Galpin, David E. Logan, and H R Krishnamurthy. Renormalization group study of capacitively coupled double quantum dots. *J. Phys.: Condens. Matter*, **18** 6545, 2006.
- [64] Martin R. Galpin, David E. Logan, and H R Krishnamurthy. Dynamics of capacitively coupled double quantum dots. *J. Phys.: Condens. Matter*, **18** 6571, 2006.
- [65] Gergely Zaránd, Chung-Hou Chung, Pascal Simon, and Matthias Vojta. Quantum criticality in a double quantum-dot system. *Phys. Rev. Lett.*, **97** 166802, 2006.
- [66] R. Žitko and J. Bonča. Enhanced conductance through side-coupled double quantum dots. *Phys. Rev. B*, **73** 035332, 2006.
- [67] Akira Oguri, Yunori Nisikawa, and A. C. Hewson. Determination of the Phase Shifts for Interacting Electrons Connected to Reservoirs. *J. Phys. Soc. Japan*, **74** 2554, 2005.
- [68] A. Oguri and A. C. Hewson. NRG approach to the transport through a finite Hubbard chain connected to reservoirs. *J. Phys. Soc. Japan*, **74** 988, 2005.
- [69] Rok Žitko and Janez Bonča. Multi-impurity Anderson model for quantum dots coupled in parallel. *Phys. Rev. B*, **74** 045312, 2006.
- [70] J. Martinek, M. Sindel, J. Barnas, J. König, G. Schon, and J. von Delft. Kondo Effect in the Presence of Itinerant-Electron Ferromagnetism Studied with the Numerical Renormalization Group Method. *Phys. Rev. Lett.*, **91** 247202, 2003.
- [71] Mahn-Soo Choi, David Sanchez, and Rosa Lopez. Kondo Effect in a Quantum Dot Coupled to Ferromagnetic Leads: A Numerical Renormalization Group Analysis. *Phys. Rev. Lett.*, **92** 056601, 2004.
- [72] W. Izumida, O. Sakai, and S. Tarucha. Tunneling through a Quantum Dot in Local Spin Singlet-Triplet Crossover Region with Kondo Effect. *Phys. Rev. Lett.*, **87** 216803, 2001.
- [73] M. Pustilnik, L. I. Glazman, and W. Hofstetter. Singlet-triplet transition in a lateral quantum dot. *Phys. Rev. B*, **68** 161303(R), 2003.
- [74] W. Hofstetter and H. Schoeller. Quantum Phase Transition in a Multilevel Dot. *Phys. Rev. Lett.*, **88** 016803, 2002.

- [75] W. Hofstetter and G. Zarand. Singlet-triplet transition in lateral quantum dots: A renormalization group study. *Phys. Rev. B*, **69** 235301, 2004.
- [76] L. Borda, G. Zaránd, W. Hofstetter, B. I. Halperin, and J. von Delft. SU(4) Fermi liquid state and spin filtering in a double quantum dot system. *Phys. Rev. Lett.*, **90** 026602, 2003.
- [77] Gabriel Kotliar. Quantum impurity models as reference systems for strongly correlated materials: the road from the Kondo impurity model to first principles electronic structure calculations with dynamical mean-field theory. *J. Phys. Soc. Japan*, **74** 147, 2005.
- [78] Antoine Georges, Gabriel Kotliar, Werner Krauth, and Marcelo J. Rozenberg. Dynamical mean-field theory of strongly correlated fermion systems and the limit of infinite dimensions. *Rev. Mod. Phys.*, **68** 13, 1996.
- [79] R. Bulla. Zero Temperature Metal-Insulator Transition in the Infinite-Dimensional Hubbard Model. *Phys. Rev. Lett.*, **83** 136, 1999.
- [80] Th. Pruschke, R. Bulla, and M. Jarrell. Low-energy scale of the periodic Anderson model. *Phys. Rev. B*, **61** 12799, 2000.
- [81] W. Koller, D. Meyer, Y. Ono, and A. C. Hewson. First- and second-order phase transitions in the Holstein-Hubbard model. *Europhys. Lett.*, **66** 559, 2004.
- [82] Gun Sang Jeon, Tae-Ho Park, Jung Hoon Han, Hyun C. Lee, and Han-Yong Choi. Dynamical mean-field theory of the Hubbard-Holstein model at half filling: Zero temperature metal-insulator and insulator-insulator transitions. *Phys. Rev. B*, **70** 125114, 2004.
- [83] Th. Pruschke and R. Bulla. Hund's coupling and the metal-insulator transition in the two-band Hubbard model. *Eur. Phys. J. B*, **44** 217, 2005.
- [84] E. Anderson, Z. Bai, C. Bischof, S. Blackford, J. Demmel, J. Dongarra, J. Du Croz, A. Greenbaum, S. Hammarling, A. McKenney, and D. Sorensen. LAPACK Users' Guide. Society for Industrial and Applied Mathematics, Philadelphia, PA, third izdaja, 1999.
- [85] Free Software Foundations. GNU General Public License. <http://www.gnu.org/copyleft/gpl.html>, 1991.
- [86] W. C. Oliveira and L. N. Oliveira. Generalized numerical renormalization-group method to calculate the thermodynamical properties of impurities in metals. *Phys. Rev. B*, **49** 11986, 1994.
- [87] W. Hofstetter. Renormalization group methods for quantum impurity systems. Disertacija, Uni. Augsburg, Germany, 2000.
- [88] F. D. M. Haldane. Theory of the atomic limit of the Anderson model: I. Perturbation expansions re-examined. *J. Phys. C: Solid State Phys.*, **11** 5015, 1978.
- [89] M. Yoshida, M. A. Whitaker, and L. N. Oliveira. Renormalization-group calculation of excitation properties for impurity models. *Phys. Rev. B*, **41** 9403, 1990.
- [90] Vivaldo L. Campo and Luiz N. Oliveira. Thermodynamics of the two-impurity Kondo model. *Phys. Rev. B*, **70** 153401, 2004.
- [91] V. L. Campo and L. N. Oliveira. Alternative discretization in the numerical renormalization group. *Phys. Rev. B*, **72** 104432, 2005.
- [92] F. D. M. Haldane. Scaling theory of the Asymmetric Anderson Model. *Phys. Rev. Lett.*, **40** 416, 1978.
- [93] M. Sindel. Numerical Renormalization Group studies of Quantum Impurity Models in the Strong Coupling Limit. Disertacija, Fak. für Physik, Ludwig-Maximilians-Universität München, 2004.
- [94] Jr. V. L. Campo and L. N. Oliveira. Renormalization-group approach to the problem of conduction through a nanostructure. *Phys. Rev. B*, **68** 035337, 2003.
- [95] Michael E. Fisher. Renormalization group theory: Its basis and formulation in statistical physics. *Rev. Mod. Phys.*, **70** 653, 1998.
- [96] Jinwu Ye. Solution of the two-channel spin-flavor Kondo model. *Phys. Rev. B*, **56** R489, 1997.
- [97] Jan von Delft, Gergely Zaránd, and Michele Fabrizio. Finite-Size Bosonization of 2-Channel Kondo model: A bridge between numerical renormalization group and conformal field theory. *Phys. Rev. Lett.*, **81** 196, 1998.
- [98] R. Bulla, A. C. Hewson, and Th. Pruschke. Numerical renormalization group calculation for the self-energy of the impurity Anderson model. *J. Phys.: Condens. Matter*, **10** 8365, 1998.
- [99] L. N. Oliveira and J. W. Wilkins. Specific heat of the Kondo model. *Phys. Rev. Lett.*, **47** 1553, 1981.
- [100] S. C. Costa, C. A. Paula, V. L. Libero, and L. N. Oliveira. Numerical renormalization-group calculation of specific heats. *Phys. Rev. B*, **55** 30, 1997.

- [101] H. O. Frota. Charge susceptibility of the spin-degenerate Anderson model. *Phys. Rev. B*, **44** 8433, 1991.
- [102] J. W. M. Pinto and H. O. Frota. Electron spin resonance of a magnetic impurity in the resonant level model. *Phys. Rev. B*, **64** 092404, 2001.
- [103] Kan Chen, C. Jayaprakash, and H. R. Krishnamurthy. Spatially dependent zero-frequency response functions and correlation functions in the Kondo model. *Phys. Rev. B*, **45** 5368, 1992.
- [104] P. W. Anderson. A poor man's derivation of scaling laws for the Kondo problem. *J. Phys. C: Solid St. Phys.*, **3** 2436, 1970.
- [105] A. A. Abrikosov and A. A. Migdal. On the theory of the Kondo effect. *J. Low Temp. Phys.*, **3** 519, 1970.
- [106] Gergely Zaránd and Jan von Delft. Analytical calculation of the finite-size crossover spectrum of the anisotropic two-channel Kondo model. *Phys. Rev. B*, **61** 6918, 2000.
- [107] Franz J. Wegner. Correction to scaling laws. *Phys. Rev. B*, **5** 4529, 1972.
- [108] A. Ramšak, J. Mravlje, R. Žitko, and J. Bonča. Spin qubits in double quantum dots: Entanglement versus the Kondo effect. *Phys. Rev. B*, **74** 241305(R), 2006.
- [109] H. O. Frota and L. N. Oliveira. Photoemission spectroscopy for the spin-degenerate Anderson model. *Phys. Rev. B*, **33** 7871, 1986.
- [110] J. J. S. Brito and H. O. Frota. Core-level photoemission spectrum for the spin-degenerate Anderson model. *Phys. Rev. B*, **42** 6378, 1990.
- [111] V. L. Libero and L. N. Oliveira. Spectral density for fermion tunneling between two centers in a metallic environment. *Phys. Rev. Lett.*, **65** 2042, 1990.
- [112] T. A. Costi and A. C. Hewson. Resistivity cross-over for the non-degenerate Anderson model. *Phil. Mag. B*, **65** 1165, 1992.
- [113] H. O. Frota and G. D. Mahan. Tunneling in fermion systems. *Phys. Rev. B*, **49** 2152, 1994.
- [114] T. A. Costi and A. C. Hewson. Transport-coefficients of the Anderson model. *J. Phys. - Cond. Mat.*, **5** L361, 1993.
- [115] T. A. Costi, A. C. Hewson, and V. Zlatic. Transport coefficients of the Anderson model via the numerical renormalization group. *J. Phys.: Condens. Matter*, **6** 2519, 1994.
- [116] T. A. Costi. Magnetotransport through a strongly interacting quantum dot. *Phys. Rev. B*, **64** 241310(R), 2001.
- [117] M. Sindel, W. Hofstetter, J. von Delft, and M. Kindermann. Frequency-dependent transport through a quantum dot in the Kondo regime. *Phys. Rev. Lett.*, **94** 196602, 2005.
- [118] G. Zaránd, L. Borda, J. von Delft, and N. Andrei. Theory of Inelastic Scattering from Magnetic Impurities. *Phys. Rev. Lett.*, **93** 107204, 2004.
- [119] R. Bulla, T. A. Costi, and D. Vollhardt. Finite-temperature numerical renormalization group study of the Mott transition. *Phys. Rev. B*, **64** 045103, 2001.
- [120] Walter Hofstetter. Generalized Numerical Renormalization Group for Dynamical Quantities. *Phys. Rev. Lett.*, **85** 1508, 2000.
- [121] F. B. Anders and A. Schiller. Real-time dynamics in Quantum Impurity Systems: A time-dependent Numerical Renormalization Group Approach. *Phys. Rev. B*, **74** 245113, 2006.
- [122] Andreas Weichselbaum and Jan von Delft. Sum-rule conserving spectral functions from the Numerical Renormalization Group. *cond-mat/0607497*, 2006.
- [123] Robert Peters, Thomas Pruschke, and Frithjof B. Anders. A numerical renormalization group approach to Green's functions for quantum impurity models. *Phys. Rev. B*, **74** 245113, 2006.